

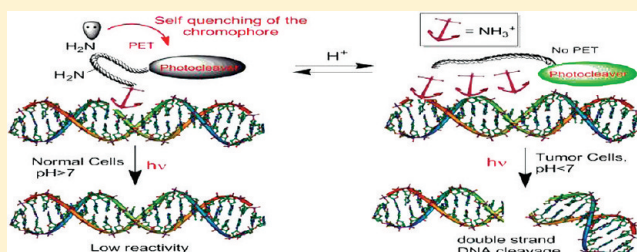
## Engineering pH-Gated Transitions for Selective and Efficient Double-Strand DNA Photocleavage in Hypoxic Tumors

Wang-Yong Yang, Saumya Roy, Boondaniwon Phrathep, Zach Rengert, Rachael Kenworthy, Diego A. R. Zorio, and Igor V. Alabugin\*

Department of Chemistry and Biochemistry, Florida State University, Tallahassee, Florida 32306-4390, United States

## Supporting Information

**ABSTRACT:** We describe a family of hybrid compounds for the most efficient light-activated double-strand (ds) DNA cleavage known to date. This family represents the second generation of “switchable” molecular systems for pH-gated ds DNA-cleavage which combine a potent DNA-photocleaver and a pH-regulated part derived from a dipeptide. Design of the pH-switchable part utilizes amino groups of different basicity. Whereas the basic amino groups are protonated throughout the biologically relevant pH range, the pH-gating amines undergo protonation at the pH threshold which separates cancer and normal cells. Control over the reactivity and selectivity is achieved via transformation of the initial protonation state (a monocation or a dication) into a trication at the acidic pH. This change leads to an extraordinary increase in the efficiency of ds DNA cleavage leading to the ds:ss ratios comparable with the most efficient nonenzymatic ds DNA cleavers. Statistical analysis reveals that these high ds:ss ratios result from the combination of several factors: (a) true double-stranded cleavage, and (b) conversion of single-stranded (ss)-scission into ds cleavage. Considerable part of ds cleavage is also produced via the combination of ss cleavage events.



## INTRODUCTION

Molecular systems, where structure, reactivity, and biological activity are “switchable” via an externally controlled factor, create new opportunities for the design of drug delivery systems,<sup>1</sup> optical sensors,<sup>2,3</sup> molecular switches/logic gate mimics,<sup>4,5</sup> and a variety of new materials.<sup>6</sup> Out of the many external stimuli, pH-gated “switching” is especially useful for addressing biochemical and environmental processes which depend on the acidity of the medium.<sup>7</sup>

In particular, the relatively acidic extracellular environment of solid tumors<sup>8,9</sup> lends itself for the design of tumor-specific pH-activated chemical agents.<sup>10</sup> Hyperglycemia and/or such drugs as amiloride, nigericin, and hydralazine, are able to lower the intracellular pH of cancer cells as well. At dosages that do not affect the normal cells, amiloride and nigericin has been reported to drop the intracellular pH in a number of tumor cell types from 7.2 to 6.2–6.6.<sup>11–14</sup> When combined with hyperglycemia and/or hypoxia, further acidification to pH as low as 5.5 is possible.<sup>15,16</sup>

One way to take advantage of these differences involves the development of pH-gated DNA cleaving agents.<sup>17</sup> The promise of DNA as a target for cancer therapy<sup>18</sup> is illustrated by the astounding biological activity of natural enediyne antibiotics. These compounds, hailed as “the most potent family of anticancer agents”,<sup>19</sup> can induce ds-DNA cleavage via abstraction of two hydrogen atoms, one from each strand of DNA duplex, with the most efficient ds DNA-cleaver from this family, calicheamicin, forming ~25–33% of ds breaks.<sup>20</sup> While

single-strand (ss) DNA damage is easily repaired by enzymatic processes,<sup>21</sup> the repair of double-strand (ds) DNA cleavage is more difficult and, thus, it can initiate self-programmed cell death, or apoptosis. Therefore, ds DNA cleavage is a more efficient tool for cancer therapy as long as it can be induced selectively in cancer cells avoiding damage to healthy cells.

Light-activated DNA-cleavers provide spatial and temporal control over DNA cleavage, allowing drug activation in the right place and at the right time, when concentration of the drug is highest in the cancer tissues.<sup>22</sup> In our previous work, we have added another level of selectivity via the development of the first pH-controlled system for ds DNA cleavage (Figure 1). This hybrid system combined an efficient DNA-cleaver capable of operating within the physiological pH range when attached to a pH-sensitive functionality.<sup>23,24</sup>

The new family of pH-dependent DNA photocleavers displayed a number of unique properties. In particular, these lysine conjugates showed efficient ds DNA cleavage (ss:ds = 2:1) rivaling the efficiency of calicheamicin,<sup>24</sup> selective cleavage at G-sites flanking AT-tracks,<sup>25</sup> and ability to convert ss DNA damage into ds DNA damage.<sup>23,26</sup> We have also shown that these compounds cleave intracellular DNA,<sup>27</sup> display light-induced cytotoxicity to several cancer cell lines,<sup>24</sup> and are susceptible to two-photon absorption (TPA) activation.<sup>28</sup>

Received: August 2, 2011

Published: November 3, 2011

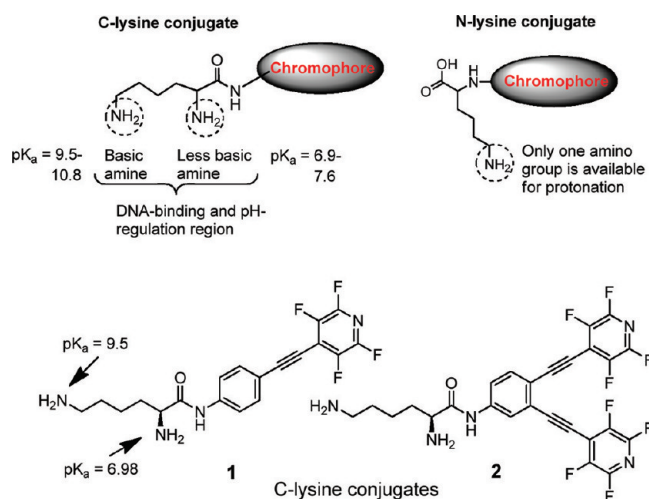


**Figure 1.** Comparison of C-lysine conjugates and N-lysine conjugates.

In this study, we describe the design and properties of light-activated systems with the ratio of *ds:ss cleavage exceeding that of calicheamicin*. Importantly, the *ds*-cleavage in such systems is suitable for selective targeting of cancer cells because this process is pH-gated: its efficiency increases dramatically at a relatively narrow and predefined pH point close to the threshold between cancerous and healthy cells.

The practical implementation of this strategy has been based on attachment of the DNA-cleaving moiety to the carboxyl group of lysine. This mode of attachment is different from a more common formation of a classic peptide bond via the  $\alpha$ -amino lysine group.<sup>29</sup> Importantly, this choice leaves both

amino groups of the lysine residue free for being included into pH-gating and facilitation of DNA-damage.

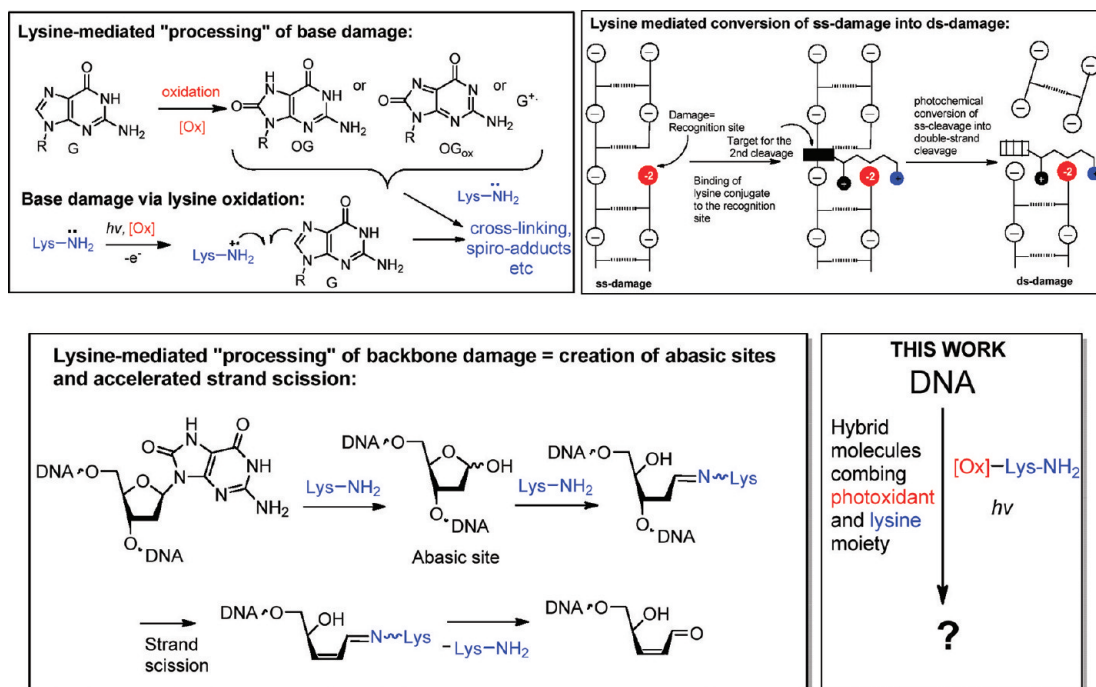
Potentially, the lysine group can interact with different forms of DNA in a variety of ways. For example, a large body of research documents the possibility of cross-link formation via a reaction with nucleobases.<sup>30</sup> Several mechanistic scenarios operate for different types of oxidative DNA-damage (e.g., 8-oxo-guanine (OG), guanine radical cation or oxidized 8-oxo-guanine (OG<sub>ox</sub>) Scheme 1).<sup>31</sup> Although the selectivity of nucleophilic attack of the lysine amino group at the oxidized DNA depends on the type of DNA damage, both C5 and C8 attacks can lead, after a rearrangement, to the formation of cross-linked spiro-adducts. Alternatively, formation of lysine-DNA adducts can also occur through initial oxidation of lysine and reaction of an N-centered radical with DNA.<sup>32</sup> This DNA-protein cross-linking can block DNA replication and, if not repaired, cause cell death.

A very interesting model for the possible role of lysine in converting OG sites into strand scission is suggested by the mechanism of action of DNA glycosylase/ $\beta$ -lyase OGG1 in which lysine acts both to displace the oxoguanine base (with the formation of an abasic site) and to promote subsequent elimination via an transient formation of a Schiff base.<sup>33</sup>

The oxidation of DNA and the formation of cross-linked products in the above examples are caused by two independent chemical agents. It is conceivable that hybrid agents which combine photooxidant and lysine would accomplish such cross-links in a more efficient manner.

The pH-gated behavior in this design is based on the different properties of these *two* amino groups.<sup>34</sup> The auxiliary amino group is protonated at a wider range of physiological conditions. This group enhances solubility of conjugates in water, increases their affinity to the negatively charged

### Scheme 1. Multiple Roles of Lysine Residues in Processing DNA Damage<sup>a</sup>



<sup>a</sup>(top left) Formation of deoxyguanosine-lysine adducts via a two-step mechanism which involves chemical or photochemical DNA oxidation followed by reaction of 8-oxoguanine with lysine.<sup>31</sup> (top right) Conversion of *ss* damage into *ds* damage.<sup>26</sup> (bottom left) Acceleration of strand scission via Schiff base formation with lysine.<sup>33</sup>

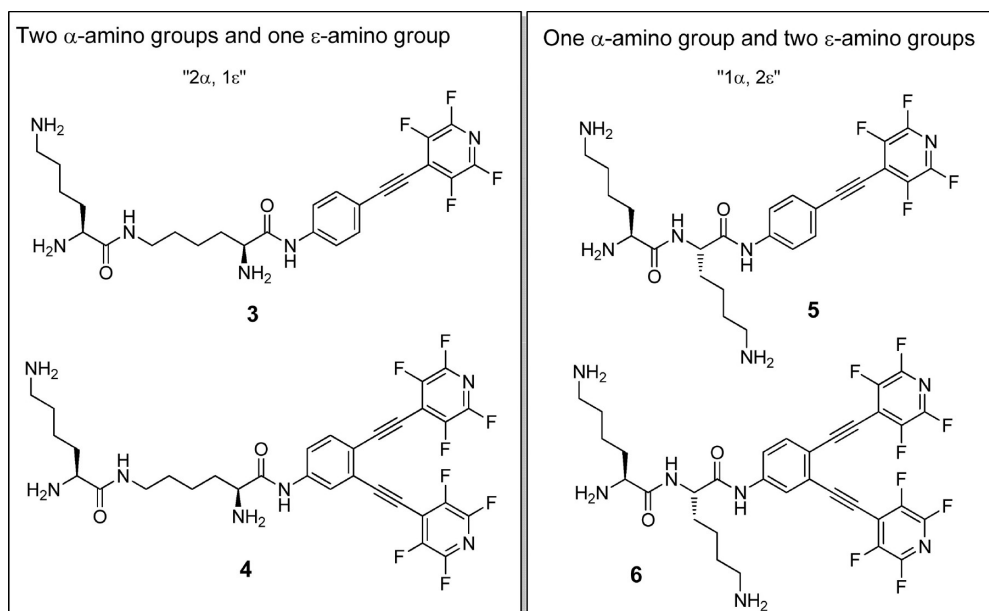


Figure 2. Structures of bis-lysine conjugates studied in this work.

backbone of DNA, and modulates the basicity of the less basic ( $pK_a \sim 7$ )  $\alpha$ -amino group. This “pH-gating” amino group undergoes protonation only under a smaller subset of conditions which enables a switch in DNA binding and photophysical properties of the conjugate at the desired pH threshold. At this threshold, the DNA-cleaver is transformed from a monocation to a dication, a change which leads to a dramatic increase in the DNA-cleaving ability.

To increase the selectivity, the difference in reactivity of the two forms should be as large as possible. A priori, one could expect that the transformation from a monocation to a trication would increase the contrast in reactivity even further. To test the possibility of designing systems activated via conversion into a multiprotonated state, we designed two types of bis-lysine peptides: one connected through a usual peptide bond via the  $\alpha$ -amino group (5, 6 in Figure 2) and the other is connected via the  $\epsilon$ -amino group (3, 4 in Figure 2).

This design also allowed us to keep the same total number of amino groups in the conjugate but vary their nature and relative basicity (two  $\alpha$ -/one  $\epsilon$ -group in 3 and 4, two  $\epsilon$ -/one  $\alpha$ -group in 5 and 6). In each of the cases, the final protonation state corresponds to a tricationic dipeptide moiety expected to display the strongest binding to DNA (Figure 3). However, the initial protonation state is expected to be different: monocationic for conjugates 3 and 4 but dicationic for conjugates 5 and 6. Because the  $\alpha$ -amino groups are responsible for the observed pH-dependence in the mono lysine conjugates, we expected that the above structural variations will have a large impact on the pH-dependence of DNA cleavage by the new bis-lysine conjugates.

## RESULTS AND DISCUSSION

**Synthesis.** The target peptide conjugates we synthesized by coupling Boc-protected lysine dipeptides (9 and 10) with anilines 7 and 8 using dicyclohexylcarbodiimide (DCC) and 1-hydroxybenzotriazole (HOBt) as coupling reagents (Scheme 2). The synthesis of anilines 7 and 8 were described previously by our group.<sup>23,24</sup> Removal of Boc-groups of compounds 11–14 with trifluoroacetic acid (TFA) in  $\text{CH}_2\text{Cl}_2$  produced the

target compounds 3–6, respectively. The final products were fully characterized by spectroscopic methods and used in the DNA-photocleavage studies as TFA salts.

**Acidity of pH-Gating Groups.** Acid–base equilibrium of  $\alpha$ -amino groups is the key to pH-gated reactivity of these compounds. To obtain accurate information about this equilibrium, we have measured the  $pK_a$  values of the three ammonium groups using fluorescence and NMR spectroscopy. The two methods differ in the type of information and amount of detail that they provide.

**Fluorescence Titrations.** Fluorescence directly reflects the protonation state of the  $\alpha$ -amino group closest to the chromophore because the donor lone pair of the chromophore can quench the chromophore excited state via electron transfer (Figure 4). Once the donor amine is protonated, this quenching mechanism is eliminated and a large increase in the fluorescence quantum yield is observed.

All pH titration experiments were carried out with only monoacetylene conjugates due to aggregation observed for the more hydrophobic enediyne conjugates at the higher pH. The pH titration with bis-lysine conjugate 3 showed only single titration curve corresponding to  $pK_a$  of 7.0. The similarity of this value to the  $pK_a$  of the  $\alpha$ -amino group of monolysine conjugate 1 (7.0) and the high efficiency of fluorescence modulation suggest that this pH titration curve corresponds to deprotonation of  $\alpha$ -ammonium group.

In contrast, the pH titration with bis-lysine conjugate 5 has two titration curves with the  $pK_a$  values of 7.1 and 10.1. Although conjugates 3 and 5 have a different number of  $\epsilon$ -ammonium groups (one for 3 and two for 5), the similarity in the first  $pK_a$  values indicates that the  $\alpha$ -amino group basicity does not depend strongly on the number of the  $\epsilon$ -amino groups. In the pH titration of compound 5, the increase in the efficiency of fluorescence quenching due the first deprotonation is less pronounced (20% vs 50% for 3), likely due to the greater distance between the chromophore and the  $\alpha$ -amino group. The relatively inefficient quenching of the excitation by the  $\alpha$ -amino group should lead to the less pronounced efficiency of pH-modulation for the di- $\epsilon$  conjugate 5. The unexpected

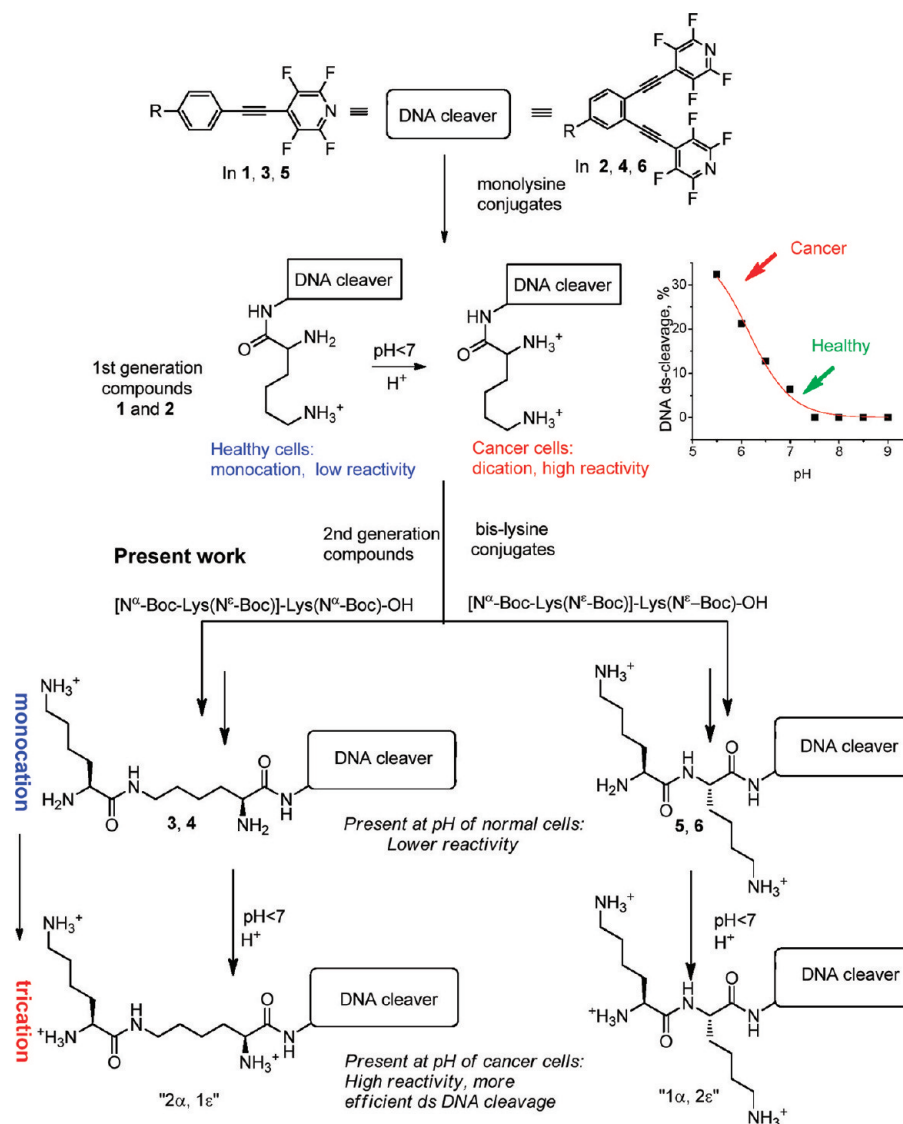


**Figure 3.** Design and structural variations for the second generation of lysine conjugates.

response of fluorescence of compound **5** to the protonation state of at least one of the two  $\epsilon$ -amino groups may indicate presence of a folded conformation in the solution where one of the remote ammonium groups participates in a cation– $\pi$  interaction with the chromophore or H-bonding with the amide group directly attached to the chromophore.

**NMR Titration.** <sup>1</sup>H NMR pH titrations provided further insight into the acid–base equilibrium of these peptide systems at the atomic resolution. This method allows independent monitoring of each of the three protonation events through observations of chemical shifts for hydrogens spatially close to each of the respective amino groups<sup>35</sup> during the pH (pD) titration (Figure 5).<sup>36,37</sup>

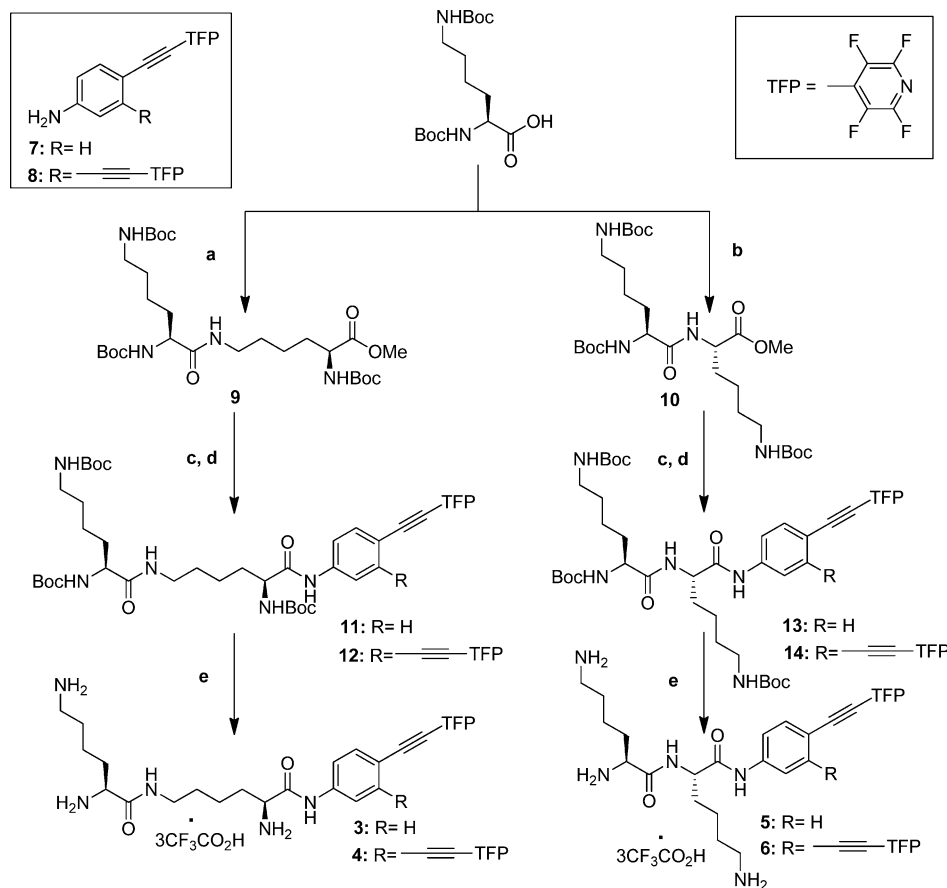
The titration curves for **3** clearly showed that two  $\alpha$ -amino groups are less basic ( $pK_a = 7.2, 7.3$ ) than the  $\epsilon$ -amino group ( $pK_a = 11.3$ ). The NMR  $pK_a$  values for **5** were 7.2 for  $\alpha$ -amino group and 10.2 for both  $\epsilon$ -amino groups (Figure 5). These  $pK_a$  values are consistent with the values from the fluorometric titrations. The close  $pK_a$  values of the two  $\alpha$ -amino groups (7.2 and 7.3) in **3** and of the two  $\epsilon$ -amino groups (10.2) in **5** indicate again that the amino group basicity in these conjugates is not strongly affected by the protonation state of other

amines, suggesting a lack of direct intramolecular interactions, e.g. H-bonding between the remote amino groups.

Interestingly, the very close  $pK_a$  values of the two  $\alpha$ -amino groups in **3** indicate that this molecule is converted from a monocation to a trication at a relatively narrow pH region between pH 7 and 8 and should respond stronger to the proton flux than the isomeric conjugate **5** (vide infra) (Table 1).

**Double-Strand Cleavage of Supercoiled DNA.** Encouraged by these results, we proceeded to investigate the pH-dependency of DNA-cleavage. Not only did both bis-lysine conjugates clearly show enhancement of DNA cleavage as a function of pH, but also the amount of ds-DNA cleavage produced by 15  $\mu$ M of mono acetylene conjugates at pH 6 (Form III/Form II ratios of 2:1 and 1:1 for di- $\alpha$  **3** and di- $\epsilon$  **5**, respectively, Figure 6) represents the highest ds:ss ratios reported in the literature, by far exceeding the analogous ratios for calicheamicin (1:2/1:3),<sup>20</sup> bleomycin (1:6–1:10)<sup>39–44</sup> and monolysine conjugates described by us earlier (1:2 at pH 6).<sup>24</sup>

The new conjugates reported in this work show significant increase in the efficiency of ds-DNA cleavage in comparison to the analogous monolysine conjugates. The correlation between the efficiency of DNA cleavage and protonation state of the

Scheme 2. Synthetic Schemes for the Preparation of Eneidyne and Acetylene Conjugates<sup>a</sup>

<sup>a</sup>Reagents and conditions: (a) Lys(*N*- $\alpha$ -Boc)-OMe, EDCl, HOBT, DIPEA, CH<sub>2</sub>Cl<sub>2</sub>; (b) Lys(*N*- $\epsilon$ -Boc)-OMe, EDCl, HOBT, DIPEA, CH<sub>2</sub>Cl<sub>2</sub>; (c) LiOH, THF:MeOH:H<sub>2</sub>O; (d) DCC, HOBT, CH<sub>2</sub>Cl<sub>2</sub>, then 7/8; (e) TFA/CH<sub>2</sub>Cl<sub>2</sub> (1:1).

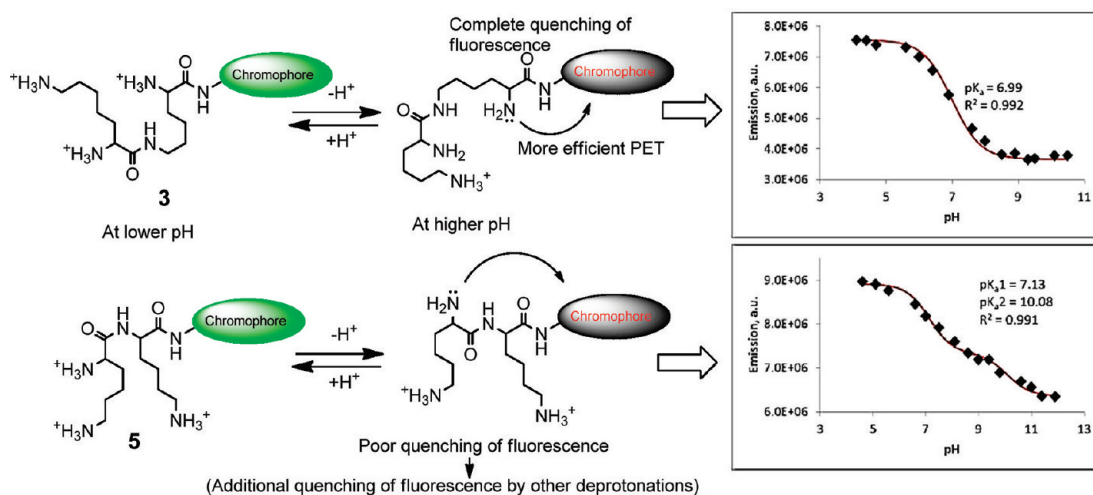


**Figure 4.** Schematic representation of electron transfer as means of quenching of fluorescence of an excited state chromophore and quantified changes in fluorescence intensity as a function of pH and their fit to the Henderson–Hasselbalch equation for acid–base equilibrium for bis-lysine di- $\alpha$  and di- $\epsilon$  conjugates 3 (top) and 5 (bottom).

dipeptide moieties illustrated by Figure 7 suggests that the tricationic form plays a particularly significant role in the ds-cleavage. Interestingly, although the correlation is observed for both the di- $\alpha$  and di- $\epsilon$  peptides, it is stronger for the less efficient di- $\epsilon$  dipeptide 5. At the lower pH, the di- $\alpha$  conjugate 3 is so efficient that further cleavage of DNA into even smaller

fragments is observed rendering the measurements less accurate and suggesting even more efficient DNA cleavage that implied by the ds:ss ratio alone. In addition, the plot of ds DNA cleavage by 5 as a function of pH fits well to the Henderson–Hasselbalch equation with 6.9 of pK<sub>a</sub> value ( $R^2 = 0.961$ ) (see the Supporting Information).

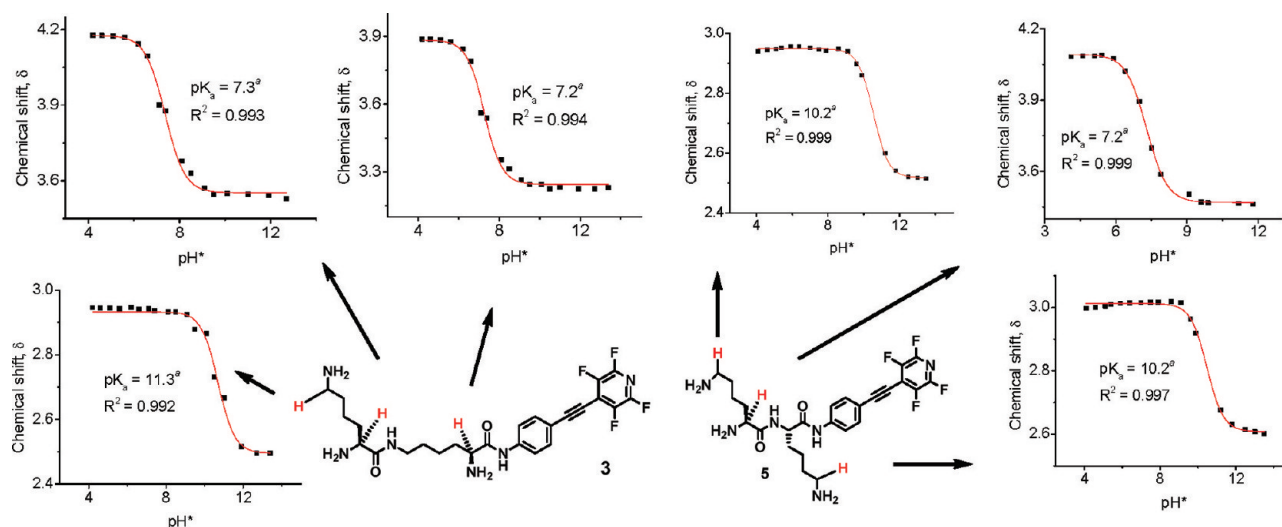


Figure 5. Chemical shift-pD titration plots for  $\alpha$ - and  $\epsilon$ -hydrogens in conjugates 3 and 5 (3 mM) in  $D_2O$ .

Table 1. The  $pK_a$  Values of Amino Groups in Conjugates 3 and 5 (The First  $pK_a$  for Lysine Conjugate 1 and Lysine Is Given for Comparison)

method	3		5		1	lysine
	emission	$^1H$ NMR <sup>a</sup>	emission	$^1H$ NMR <sup>a</sup>	emission	
$pK_{a1}$	7.0	7.2	7.1	7.2	7.0	8.95 <sup>b</sup>
$pK_{a2}$		7.3	10.1	10.2		10.53 <sup>b</sup>
$pK_{a3}$		11.3		10.2		

<sup>a</sup>Data include a correction factor from ref 36. <sup>b</sup>Data from ref 38.

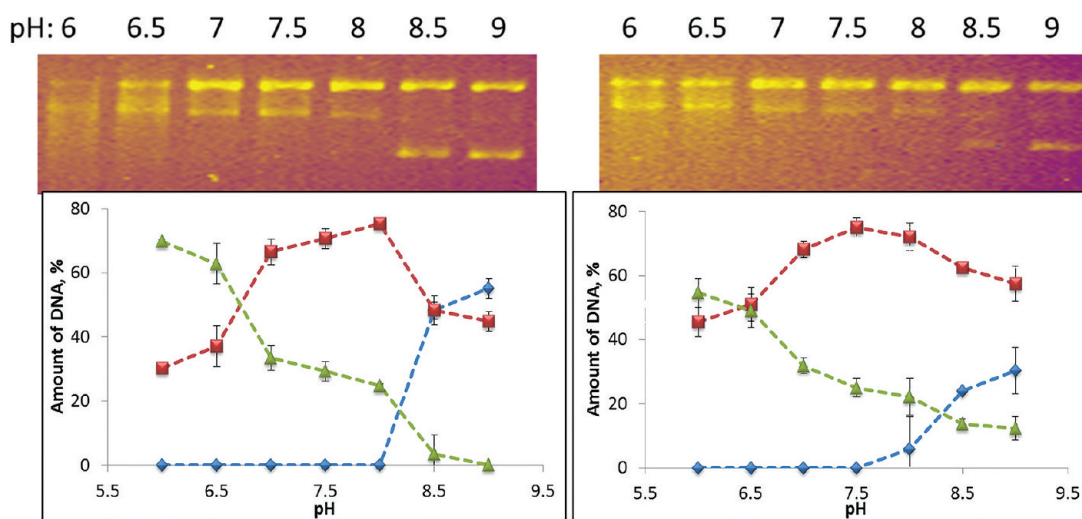
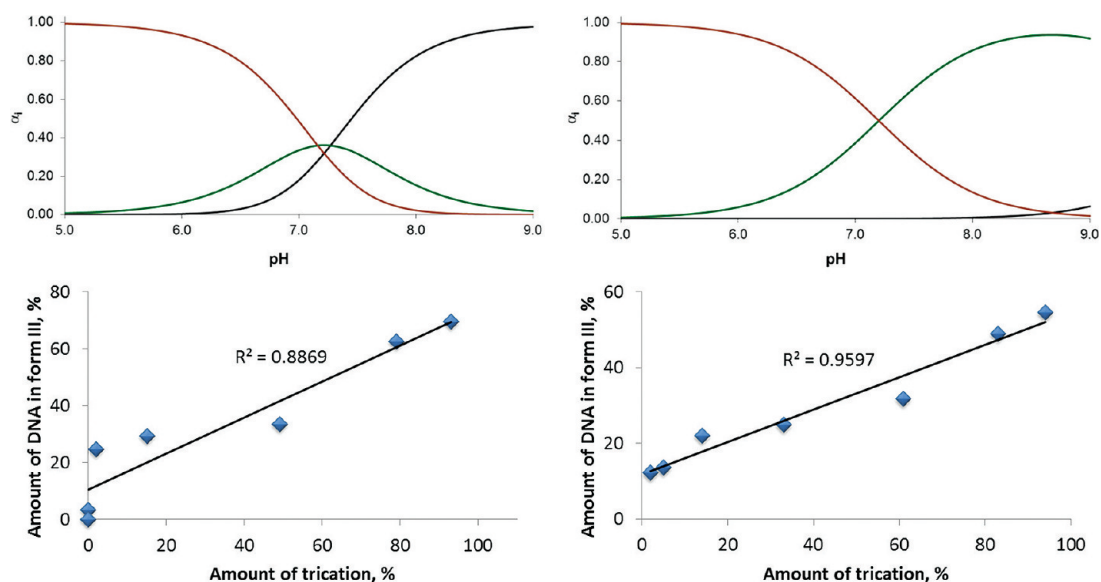


Figure 6. (top) Quantified cleavage data for plasmid relaxation assay for DNA photocleavage with 15  $\mu M$  of acetylenic conjugates 3 (left) and 5 (right) and 38  $\mu M$  (bp) of pBR322 plasmid DNA at pH range of 6–9 after 10 min of UV (>300 nm) irradiation. Reported values represent the average of three experiments. Code: form I, blue diamond; form II, red square; form III, green triangle.

Although the chemical mechanism for the DNA cleavage and the possibility of DNA alkylation and DNA-lysine cross-linking are under investigation at this point, the new conjugates reported in this work unambiguously show significant increase in the efficiency of DNA cleavage promoted by a change from a monolysine to a bis-lysine moiety. Surprisingly, significant DNA cleavage including some ds DNA cleavage is observed even at pH 8, the conditions where the monolysine conjugates do not cause this damage in appreciable amounts. This observation suggests that bis-lysine acetylene conjugates are

overall more efficient DNA cleavers than their monolysine conjugates.

By using the statistical test of Povirk,<sup>45</sup> one can gain more insight into the nature of the cleavage as long as there is a set condition where all of the three DNA forms are present.<sup>46</sup> This test assumes a Poisson distribution of strand cuts and calculates the average number of ss- ( $n_1$ ) and ds-breaks ( $n_2$ ) per DNA molecule. As we observed complete disappearance of supercoiled DNA after 10 min of irradiation in both the cases for compound 3 as well as compound 5, we performed the DNA-



**Figure 7.** Relative amounts of mono- (black), di- (green), and tricationic (red) forms as function of pH (top) and correlation of DNA ds-cleavage with the trication mole fraction (bottom) for conjugates **3** (left) and **5** (right).

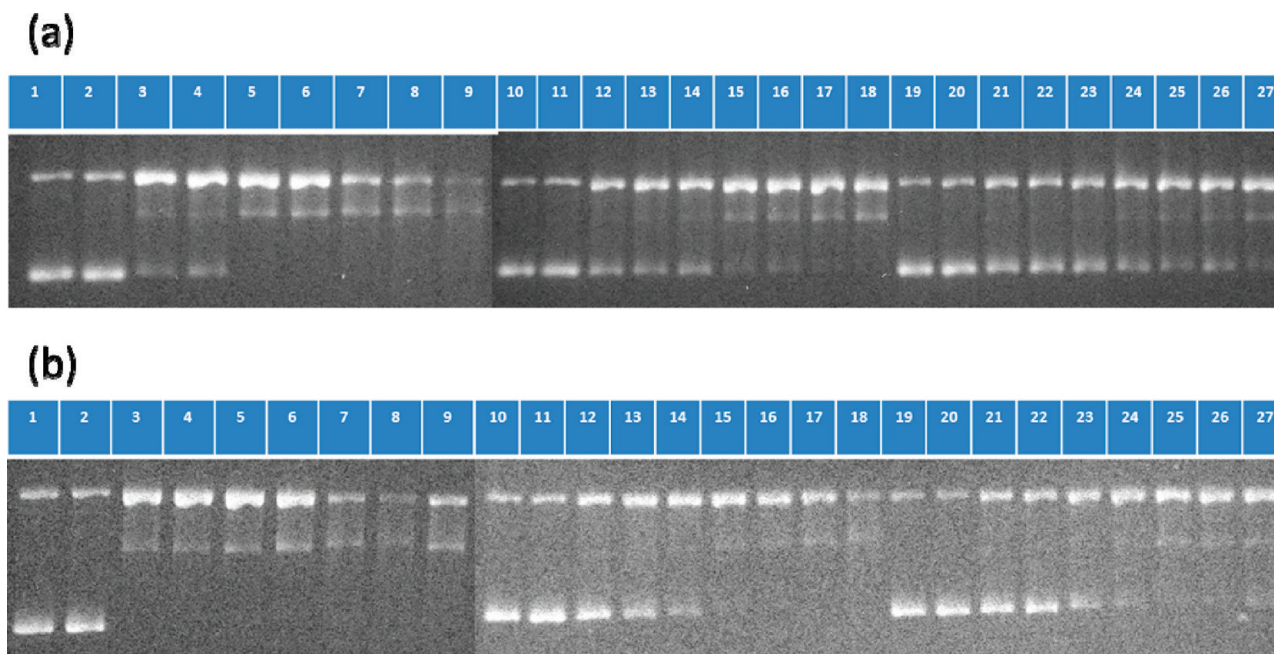


**Figure 8.** Photochemical cleavage of pBR322 plasmid DNA (38  $\mu\text{M}$ /bp) by (a) **3** (15  $\mu\text{M}$ ) and (b) **5** (15  $\mu\text{M}$ ) in phosphate buffer (20 mM). Lane 1, DNA+hv for 10 min; lanes 2–9, DNA + **3/5** + hv for 0, 0.5, 1, 2, 4, 6, 8, and 10 min of irradiation (>300 nm) respectively at pH 6.0. Lane 10, DNA+hv for 10 min; lanes 11–18, DNA + **3/5** + hv for 0, 0.5, 1, 2, 4, 6, 8, and 10 min of irradiation respectively at pH 7.0. Lane 19, DNA+hv for 10 min; lanes 20–27, DNA + **3/5** + hv for 0, 0.5, 1, 2, 4, 6, 8, and 10 min of irradiation respectively at pH 8.0.

photocleavage experiment as a function of irradiation time at the pH conditions 6, 7, and 8 (Figure 8).

It is not possible to calculate the  $n_1/n_2$  ratio for those times where there is no supercoiled DNA present or no ds-cleavage was found. For the conjugate **3** at pH 6, less than 17% supercoiled DNA remains after 2 min irradiation and  $n_1/n_2$  values could not be calculated for irradiation time longer than 2 min (Figure 9). The  $n_1/n_2$  ratios at pH 6 slightly decrease with the irradiation time, but there is not enough data to be certain that this trend persists. Data showed low  $n_1/n_2$  ratio at pH 7 which decreases further with time (from 4.4 at 2 min to 2.2 after 10 min) (Table 2). These data suggests the likeliness of

efficient ds-cleavage at pH 6 but the full statistical analysis is impossible at the longer times due to disappearance of supercoiled DNA. Compound **5** also displayed the high ds-cleavage at pH 6.0, although it is less selective than compound **3** (see Supporting Information for quantitative analysis).

Because of the high reactivity of the conjugates, no supercoiled DNA remained after 30 s of irradiation for compound **5** in pH 6 at 15  $\mu\text{M}$  concentration (Figure 10). Lowering the concentration to 10  $\mu\text{M}$  produced less DNA cleavage, but due to absence of all the three DNA form in a single lane it was impossible to calculate the  $n_1/n_2$  ratio.

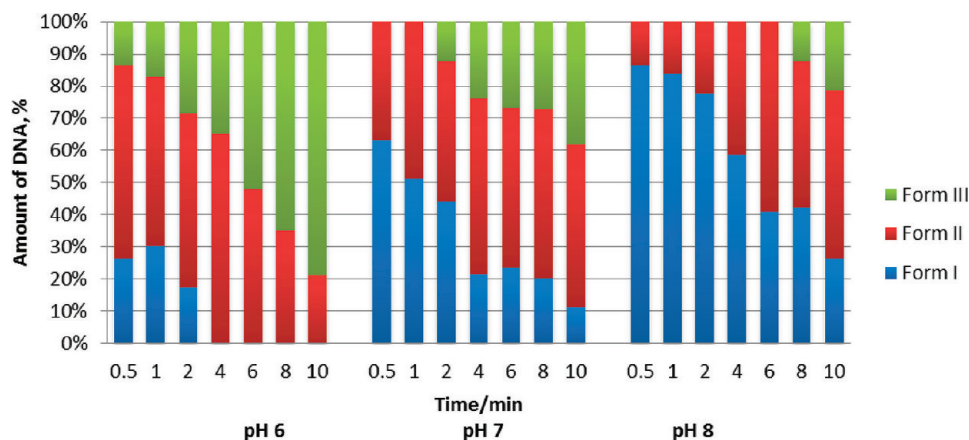


Figure 9. Quantified data of plasmid relaxation assays with 15  $\mu\text{M}$  of mono acetylene conjugate 3.

Table 2. Statistical Analysis of the Single-Strand and Double-Strand Break Formation by 3 as a Function of Irradiation Time at pH 6.0, 7.0, and 8.0<sup>a</sup>

time/min	relative amounts (%) at pH 6.0			no. of ss-breaks ( $n_1$ ) and ds-breaks ( $n_2$ ) per molecule		
	form I	form II	form III	$n_1$	$n_2$	$n_1/n_2$
0.5	26.5	60.0	13.5	1.17	0.16	7.5
1	30.2	52.7	17.1	0.99	0.21	4.8
2	17.3	54.2	28.4	1.36	0.40	3.4
4	0.0	65.1	34.9		0.54	
6	0.0	48.1	51.9		1.08	
8	0.0	35.0	65.0		1.85	
10	0.0	21.3	78.7		3.69	

time/min	relative amounts (%) at pH 7.0			no. of ss-breaks ( $n_1$ ) and ds-breaks ( $n_2$ ) per molecule		
	form I	form II	form III	$n_1$	$n_2$	$n_1/n_2$
0.5	64.6	35.4	0.0	0.44	0.00	
1	52.7	47.3	0.0	0.64	0.00	
2	45.8	41.5	12.7	0.64	0.15	4.4
4	22.6	52.4	25.0	1.15	0.33	3.5
6	24.7	47.2	28.1	1.01	0.39	2.6
8	20.9	51.0	28.1	1.17	0.39	3.0
10	11.7	47.8	40.5	1.47	0.68	2.2

time/min	relative amounts (%) at pH 8.0			no. of ss-breaks ( $n_1$ ) and ds-breaks ( $n_2$ ) per molecule		
	form I	form II	form III	$n_1$	$n_2$	$n_1/n_2$
0.5	86.4	13.6	0.0	0.15	0	
1	83.9	16.1	0.0	0.18	0	
2	77.8	22.2	0.0	0.25	0	
4	58.6	41.4	0.0	0.00	0	
6	40.8	59.2	0.0	0.90	0	
8	42.3	45.6	12.1	0.72	0.14	5.3
10	26.3	52.3	21.3	1.06	0.27	3.9

<sup>a</sup>Amount of form II DNA was calculated by deducting the amount of form I DNA present in the control experiment at irradiation time = 0 (22%). See the Supporting Information for the calculated  $n_1/n_2$  ratios without this correction.

These data suggests that the high Form III/Form II ratios result, at least partially, from the combination of very efficient multiple ss-scission. The decreasing  $n_1/n_2$  ratio also suggests that conversion of ss-damage into ds-damage may also occur as described in Scheme 1.

The additional concentration effects on the efficiency of DNA cleavage are summarized in Figure 11. At pH 6, the total

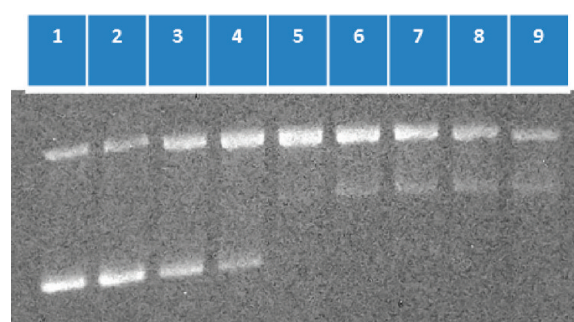
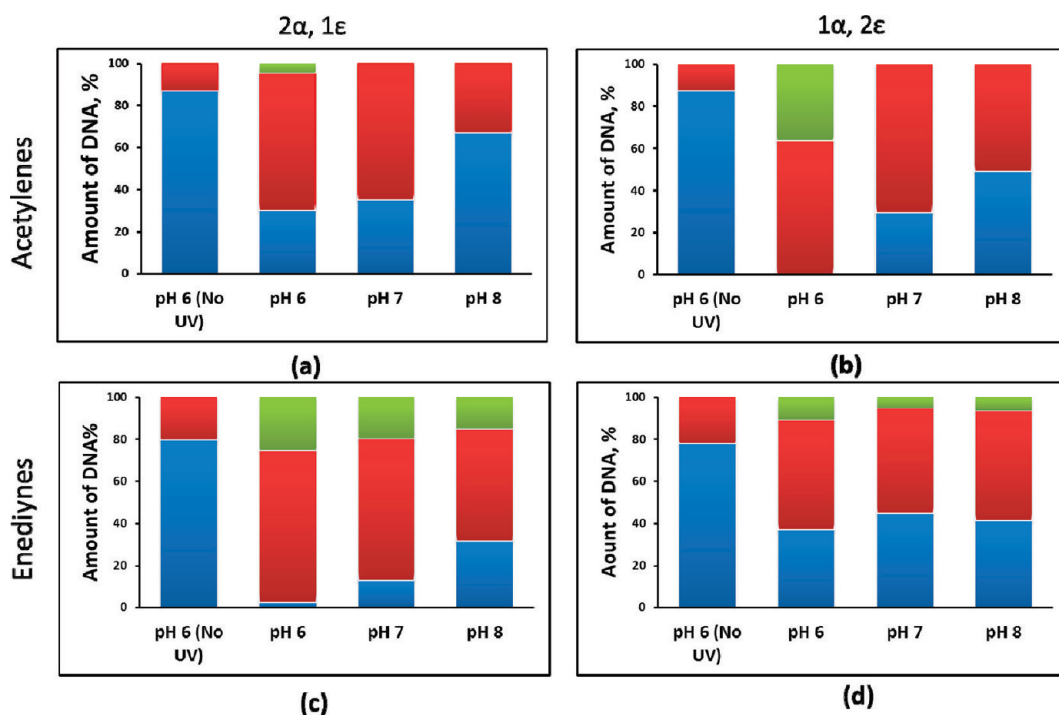


Figure 10. Photochemical cleavage of pBR322 supercoiled DNA (38  $\mu\text{M}/\text{bp}$ ) by 5 (10  $\mu\text{M}$ ) in phosphate buffer (20 mM). Lane 1, DNA +  $h\nu$  for 10 min; lanes 2–9, DNA + 5 +  $h\nu$  for 0, 0.5, 1, 2, 4, 6, 8, and 10 min of irradiation (>300 nm), respectively, at pH 6.0.

percentage of DNA cleavage decreases from 155% (200% cleavage corresponds to full conversion of supercoiled DNA to linear DNA = full ds DNA cleavage) to 136% to 32% for conjugate 5 and from 159% to 75% to 50% for conjugate 3 (upon 15  $\rightarrow$  10  $\rightarrow$  5  $\mu\text{M}$  changes, data for the 10  $\mu\text{M}$  concentrations are shown in Figure 11-1). Although the concentration effects are significant for both mono acetylene conjugates, the acetylene conjugate 3 with two  $\alpha$ - and one  $\epsilon$ -amino groups is affected by the concentration change much more than the isomeric bis-lysine conjugate 5, which has two  $\epsilon$ -amino groups available (Figure 11a). These results suggests that, although  $\alpha$ -amino groups play the key role in pH-regulation, the  $\epsilon$ -amino groups which are analogous to amino groups in the histone proteins may be important for further “processing” of the oxidative DNA damage, possibly with the involvement of processes outlined in Scheme 1. In addition, the greater fluorescence enhancement upon the binding of conjugate 5 to DNA relative to that for compound 3 (both at pH 6) suggests that the chromophore moiety of 5 is placed deeper inside of the hydrophobic environment of DNA at the lower pH. The tighter binding of compound 3 in its tricationic state can also be partially responsible for the relative insensitivity of its DNA cleavage to the secondary factors.

At 10  $\mu\text{M}$  concentration, both the full cleavage of supercoiled DNA and the appearance of ds cleavage (average ss/ds ratio of 1.7:1, Figure 11b) by the “1 $\alpha$ ,2 $\epsilon$ ” conjugate 5 were observed only at pH 6. At pH 7, ~40% of supercoiled DNA remained intact and no ds-damage was detected (~50% of supercoiled DNA was intact at pH 8). The particularly large increase in the



**Figure 11.** Quantified data of plasmid relaxation assays with 10  $\mu\text{M}$  of mono acetylene conjugate 3 and 5 (a and b) and 10  $\mu\text{M}$  of enediyne conjugates 4 and 6 (c and d). Reported values represent the average of four experiments.

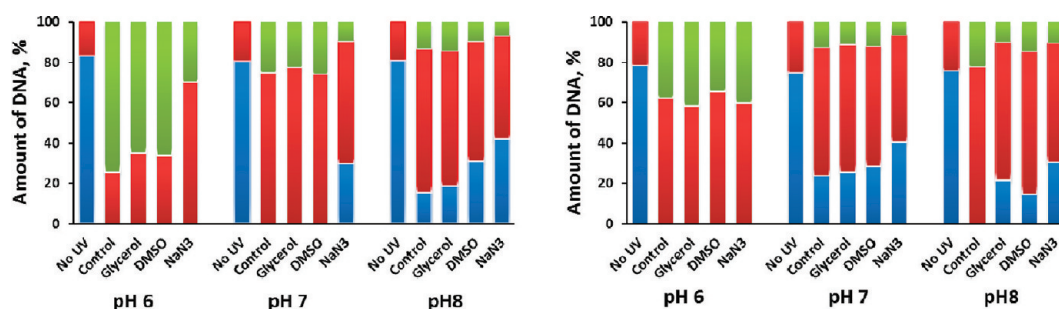


**Figure 12.** Effect of hydroxyl radical/singlet oxygen scavengers (20 mM) upon the efficiency of DNA cleavage at pH 6, 7, and 8 by 15  $\mu\text{M}$  of 3 (left) and 15  $\mu\text{M}$  of 5 (right) after 10 min irradiation. Color coding: blue, form I; red, form II; green, form III.

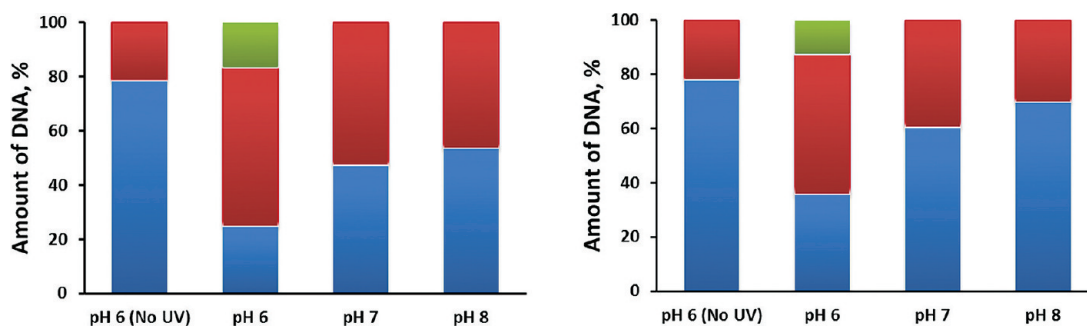


**Figure 13.** Quantified data of plasmid relaxation assays with 5  $\mu\text{M}$  of enediyne conjugates 4 (left) and 6 (right).

total percentage of DNA cleavage at the threshold separating acidified and normal tissues (136% (pH 6)  $\gg$  61% (pH 7)) is promising for selective targeting of acidic cancers.

The differences between conjugates 3 and 5 in regards to the chemical mechanism of the DNA cleavage were further illustrated by the effects of common scavengers for hydroxyl radical (glycerol, DMSO)<sup>47</sup> and singlet oxygen (NaN<sub>3</sub>)<sup>48</sup> in the plasmid relaxation assays (Figure 12). While the protecting

effect by glycerol and DMSO was small, the protection of DNA cleavage by NaN<sub>3</sub> was noticeable with both conjugates, except for the "2ε,1α" conjugate 5 at pH 6. Failure of scavengers to prevent DNA cleavage at these conditions is, again, consistent with the relatively tight binding and a direct mechanism for DNA modification by conjugate 5.

Enediyne conjugates showed a different DNA cleavage pattern (Figure 13c,d) in comparison with the mono acetylene

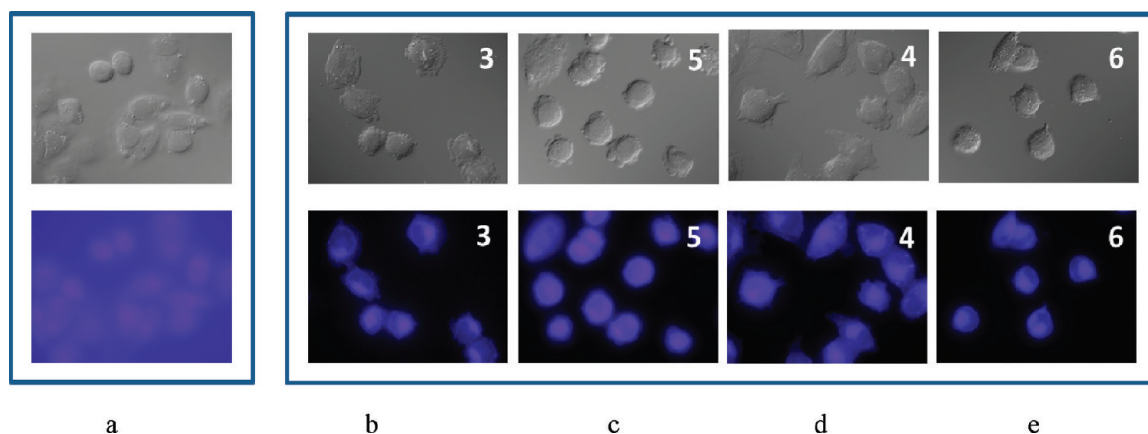


**Figure 14.** DIC (top) and fluorescence (bottom) cell images of A375 cells without compound (a) and with 30  $\mu\text{M}$  of 3 (b), 4 (c), 5 (d), and 6 (e) at pH 7.4 (compound numbers are also shown in the top right corners of the images).

conjugates. First, efficient photoreactivity is observed at the lower concentrations. At pH 6, 17% and 13% of ds DNA cleavage was observed, respectively, for the enediyne conjugates 4 and 6 at concentrations as low as 5  $\mu\text{M}$  (Figure 13). At this concentration, 92% and 77% of total DNA damage by 4 and 6 compare favorably with the total damage by 10  $\mu\text{M}$  of mono acetylene conjugate 5 in Figure 13. However, in spite of the efficient ds DNA cleavage of enediyne conjugates at the lower concentration, there was no big increase in DNA damage at 10  $\mu\text{M}$ . We attribute this unexpected result to the aggregation of enediyne conjugates which have more hydrophobic core.<sup>49</sup> Interestingly, with 10  $\mu\text{M}$  of enediynes, ds DNA cleavage was observed at all pH conditions including pH 8. This observation indicates that enediyne conjugates may have another mechanism of DNA damage which is not concentration-dependent (at least, for ds DNA cleavage) and less pH-dependent overall. More detailed studies of the chemical mechanism responsible for the highly efficient DNA cleavage are needed, but photo C1–C5 cyclization of TFP-substituted enediynes to the corresponding indenenes involves the net transfer of four hydrogen atoms from the environment,<sup>50</sup> which may be responsible for the different photoreactivity of enediyne conjugates.

Absence of ds damage at pH 7 at the 5  $\mu\text{M}$  concentration of enediynes 4 and 6 is particularly encouraging from a practical perspective. The differences in the efficiency and pH-dependence of DNA cleavage by enediynes have two probable origins. Our earlier work suggested that enediyne and acetylene conjugates often bind DNA in a different way (e.g., intercalation vs groove binding)<sup>24</sup> and also may cause DNA damage via different mechanisms, e.g., C1–C5 cyclization vs alkylation.<sup>51</sup>

**Cellular Uptake of Bis-lysine Conjugates, Intracellular DNA Damage, and Cell Proliferation Studies.** Experimental data (both the differential interference contrast (DIC) and fluorescence cell images) displaying uptake bis-lysine conjugates by melanoma cells are given in Figure 14–4. Whereas no significant fluorescence was detected from the cells without conjugates (Figure 14a), the cells became fluorescent after 30 min incubation with the conjugates, (Figure 14b,c,d,e), indicating that all four conjugates can penetrate the cellular membrane. The fluorescence is relatively well-distributed throughout the whole cell suggesting that the bis-lysine conjugates are capable of entering the nuclei as well.

To test the DNA damaging ability of the conjugates in cells, we performed single-cell gel electrophoresis (SCGE) assay. The control SCGE assay results for undamaged cells and commercially obtained cells with DNA damage are given for comparison (Figure 15a,b). SCGE assay with healthy cells

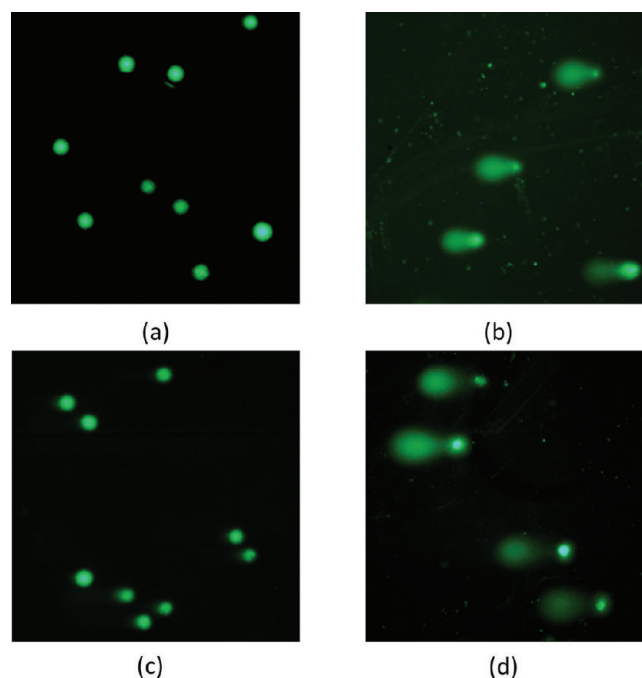


**Figure 15.** Images of SCGE assays. (a) Undamaged control cells; (b) control cells with damaged DNA; (c) no compound + UV; (d) A375 cells + UV + compound 3.

showed no tails indicative of DNA damage (Figure 15a), whereas the damaged cells produced the characteristic tails, the size of which correlates with the amount of DNA damage in these cells (Figure 15b).

Experiments evaluating light-induced DNA damage in melanoma cells are summarized in Figure 15c,d. In the absence of the photoactivated conjugates, irradiation for 10 min does not produce efficient DNA damage (Figure 15c). In contrast, photochemical activation of compound 5 produced very efficient intracellular DNA damage in the A375 cells (Figure 15d). These results confirm that compound 5 can penetrate

into the cancer cell nucleus and damage highly compacted DNA upon photoactivation.

To further elucidate the cellular effects of these compounds, we tested their ability to cause DNA damage in A375 melanoma cells. Figure 16 (left) showed that the conjugate 5

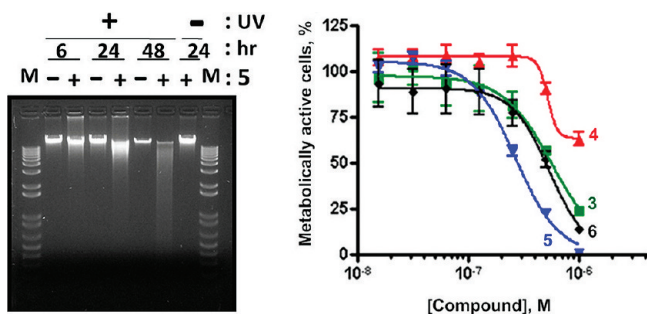


**Figure 16.** (left) UV activated compound KK (1a,2e)-Ac (5) causes DNA damage in A375 cells. A375 cells were treated as described in the Experimental Section. After UV irradiation cells were harvested at 6, 24, and 48 h, DNA was extracted and analyzed by gel electrophoresis. Smaller – and + symbols indicates absence or presence of conjugate 5. Time points are indicated by numbers in hours; M stands for DNA marker. Bigger – and + indicates whether cells were UV irradiated (20 min). (right) Cell proliferation assay using human melanoma A375 cell line with compound 3 (green squares), 4 (red triangles pointing up), 5 (blue triangles pointing down), and 6 (black diamonds) after 10 min of irradiation at 360 nm. The cell counts were normalized to the experiment with UV irradiation.

had the ability to target and cause DNA damage in a UV dependent manner. DNA degradation was observed at all-time points, and it also progressively increased with time. The continuous increase in DNA degradation is considered as one of the signs of apoptosis due to the release of endogenous endonucleases,<sup>52</sup> whereas the appearance of fragmented DNA on the gel was similar to that reported earlier by Wyllie and co-workers for the fraction of apoptotic cell lysates which has been cross-linked to the nucleus with the involvement of histone proteins.<sup>53</sup>

Finally, we investigated phototoxicity of the four conjugates against the melanoma cells. Gratifyingly, all four conjugates (3, 4, 5, and 6) are inactive in the dark and do not inhibit cell proliferation at the concentration <10  $\mu$ M (see the Supporting Information). On the other hand, all the conjugates displayed photoinduced cytotoxicity against this cancer cell line at the submicromolar levels. Conjugate 5 displayed a particularly strong phototoxicity toward the human melanoma A375 cell line at the nanomolar range ( $CC_{50} = 2.7 \times 10^{-7}$  M after 10 min of irradiation using 360 nm light) (Figure 16).

## CONCLUSION

In conclusion, this work describes the second generation of pH-gated hybrid molecules which produces the most efficient light-activated double-strand DNA cleavage known to date. These hybrid compounds consist of two functional parts: an efficient DNA-photocleaving agent and a pH-regulated part derived from a basic dipeptide (bis-lysine). In the design of the pH-switchable part, we took advantage of the different basicity of  $\alpha$ - and  $\epsilon$ -amino groups of lysine. The more basic  $\epsilon$ -amino groups are protonated throughout all biologically relevant pH range, whereas the  $\alpha$ -amino groups undergo selective protonation at the desired pH threshold which separates cancer and normal

cells. This protonation leads to the extraordinary increase in reactivity under the conditions suitable for selective targeting of cancer cells.

The two alternative approaches to the construction of the dipeptide moiety allowed us to change the relative number of the  $\alpha$ -amino vs  $\epsilon$ -amino groups and achieve better control over the reactivity and selectivity of the ds DNA cleavage. Depending on the structure, the conjugates exist as either monocations or dications at the neutral pH but are transformed into trications at the acidic pH. The efficiency of ds-cleavage is increased dramatically at the slightly acidic pH (<7), where it exceeds the ds:ss ratio of calicheamicin. We have also demonstrated that these conjugates are also capable of the efficient penetration through cellular membranes and induction of intracellular DNA damage. The high phototoxicity displayed toward melanoma cells with  $CC_{50}$  in the 10<sup>-7</sup> M range suggests that this class of hybrid molecules has potential value for the development of future light-activated anticancer agents.

## EXPERIMENTAL SECTION

**General Information.** <sup>1</sup>H, <sup>13</sup>C NMR spectra were collected on a Bruker 400 and 600 MHz NMR spectrometer. Mass spectrometry data was collected on a Jeol JMS-600H. UV spectra were recorded on a Shimadzu UV-2100. Fluorescence spectra were obtained with SPEX FluorMax spectrofluorimeter using right-angle geometry. pH was adjusted with AB 15 plus pH meter (Accument) after standardization at 25 °C. All buffers were prepared and pH-adjusted at room temperature (25 °C). Purity of biologically important compounds is  $\geq 95\%$ . Reagent kit for single cell gel electrophoresis assay kit, CometAssay, and control cells containing different levels of DNA damage, CometAssay Control Cell, were purchased from Trevigen, Inc. The CC0 sample corresponds to cells with undamaged DNA.<sup>54</sup> Miligel FisherBiotech Horizontal Electrophoresis System was used for electrophoresis. An Olympus BX61 microscope attached with the DP71 color digital camera was used to take fluorescence images of SCGE assay.

### (S)-Methyl 6-((S)-2,6-Bis((tert-butoxycarbonyl)amino)hexanamido)-2-((tert-butoxycarbonyl)amino)hexanoate (9).

The acid, Boc-L-lysine-OH (550 mg, 1.52 mmol) was dissolved in CH<sub>2</sub>Cl<sub>2</sub> (10 mL) and cooled to 0 °C. Then it was sequentially treated with HOBt (308 mg, 2.28 mmol) and EDCI (436 mg, 2.28 mmol). After 15 min, amine Lys(N- $\alpha$ -Boc)-OMe (475 mg, 1.82 mmol) was added to the reaction mixture followed by DIPEA (0.8 mL, 4.56 mmol). After stirring for 12 h at room temperature, the reaction mixture was extracted with ethyl acetate, washed with saturated NH<sub>4</sub>Cl solution, water, brine, dried (Na<sub>2</sub>SO<sub>4</sub>), filtered, and concentrated in vacuo. Chromatographic purification (SiO<sub>2</sub>, 30% ethyl acetate in hexane eluant) of the residue provided dipeptide 9 (700 mg, 81%) as white solid. <sup>1</sup>H NMR (400 MHz, CDCl<sub>3</sub>):  $\delta$  6.23 (bs, 1H), 5.28 (bs, 1H), 4.63 (bs, 1H), 4.24 (m, 1H), 4.03–3.95 (m, 1H), 3.73 (s, 3H), 3.33–3.16 (m, 2H), 3.10 (dd,  $J = 13.0, 6.7$  Hz, 2H), 1.89–1.73 (m, 2H), 1.73–1.57 (m, 4H), 1.56–1.29 (m, 33H). <sup>13</sup>C NMR (100 MHz, CDCl<sub>3</sub>):  $\delta$  173.3, 172.4, 156.1, 155.8, 155.5, 79.7, 78.9, 54.2, 53.4, 53.2, 52.1, 39.9, 38.7, 32.2, 31.8, 29.5, 28.9, 28.4, 28.3, 22.6. MS (ESI):  $m/z$  (%) 611 (100) [M + Na]<sup>+</sup>, 589 (20) [M + H]<sup>+</sup>. HRMS (ESI): calcd for C<sub>28</sub>H<sub>52</sub>N<sub>4</sub>O<sub>9</sub>Na [M + Na]<sup>+</sup> 611.36320, found 611.36505.

### (S)-Methyl 2-((S)-2,6-Bis((tert-butoxycarbonyl)amino)hexanamido)-6-((tert-butoxycarbonyl)amino)hexanoate (10).

The dipeptide 10 was prepared by using the same procedure as synthesis of compound 9 in 90% yield. <sup>1</sup>H NMR (400 MHz, CDCl<sub>3</sub>):  $\delta$  6.65 (d,  $J = 7.7$  Hz, 1H), 5.21 (bs, 1H), 4.69 (bs, 1H), 4.62–4.53 (m, 1H), 4.12–4.03 (m, 1H), 3.73 (s, 3H), 3.17–3.03 (m, 4H), 1.91–1.78 (m, 2H), 1.75–1.57 (m, 3H), 1.55–1.24 (m, 34H). <sup>13</sup>C NMR (100 MHz, CDCl<sub>3</sub>):  $\delta$  172.6, 172.2, 156.2, 156.1, 155.8, 79.9, 79.0, 54.2, 52.3, 51.8, 40.1, 39.8, 31.9, 31.7, 29.5, 29.3, 28.4, 28.3, 22.4. MS (ESI):  $m/z$  (%) 611 (100) [M + Na]<sup>+</sup>. HRMS (ESI): calcd for C<sub>28</sub>H<sub>52</sub>N<sub>4</sub>O<sub>9</sub>Na [M + Na]<sup>+</sup> 611.36320, found 611.36283.

**tert-Butyl N-[(1S)-5-[(2S)-2,6-Bis(tert-butoxycarbonylamino)hexanoyl]amino]-1-[4-[2-(2,3,5,6-tetrafluoro-4-pyridyl)ethynyl]phenyl]carbamoyl]pentyl]carbamate (11).** To a solution of dipeptide 9 (300 mg, 0.522 mmol) in THF:MeOH:H<sub>2</sub>O (3:1:1, 5 mL) at 0 °C, LiOH·H<sub>2</sub>O (65 mg, 2.40 mmol) was added and stirred at the room temperature for 3 h. The reaction mixture was then acidified to pH 2 with 1N HCl. It was extracted with ethyl acetate, washed with brine, dried (Na<sub>2</sub>SO<sub>4</sub>), filtered, and concentrated in vacuo to get the crude acid.

The above prepared crude acid was dissolved in CH<sub>2</sub>Cl<sub>2</sub> (10 mL) and cooled to 0 °C. It was sequentially treated with HOBt (105 mg, 0.783 mmol) and DCC (161 mg, 0.783 mmol). After 15 min, amine 7 (205 mg, 0.783 mmol) was added to the reaction mixture and stirred for 12 h, raising the temperature to rt. The reaction mixture was extracted with ethyl acetate, washed with saturated NH<sub>4</sub>Cl solution, saturated NaHCO<sub>3</sub>, 1 N HCl, water, brine, dried (Na<sub>2</sub>SO<sub>4</sub>), filtered, and concentrated in vacuo. Chromatographic purification (SiO<sub>2</sub>, 50% ethyl acetate in hexane eluant) of the residue provided compound 11 (258 mg, 60%) as yellow solid. <sup>1</sup>H NMR (400 MHz, CDCl<sub>3</sub>): δ 9.12 (bs, 1H), 7.65 (d, d, J = 8.6 Hz, 2H), 7.56 (d, J = 8.6 Hz, 2H), 6.51 (bs, 1H), 5.62 (bs, 1H), 5.31 (bs, 1H), 4.66 (bs, 1H), 4.25–4.13 (m, 1H), 4.09–3.99 (m, 1H), 3.52–2.97 (m, 4H), 1.98–1.89 (m, 1H), 1.87–1.78 (m, 1H), 1.77–1.62 (m, 4H), 1.61–1.30 (m, 33H). <sup>13</sup>C NMR (100 MHz, CDCl<sub>3</sub>): δ 172.8, 171.3, 156.3, 143.5 (dm, J = 245 Hz), 141.7 (dm, J = 264 Hz), 133.3, 119.6, 117.6, 115.5, 107.0, 80.6, 80.2, 79.2, 73.2, 55.1, 54.5, 49.2, 39.9, 33.9, 29.7, 28.8, 28.5, 28.4, 25.6, 24.9, 22.7, 22.6. MS (ESI): m/z (%) 845 (100) [M + Na]<sup>+</sup>. HRMS (ESI): calcd for C<sub>40</sub>H<sub>34</sub>F<sub>4</sub>N<sub>6</sub>O<sub>8</sub>Na [M + Na]<sup>+</sup> 845.38369, found 845.38406.

**(S)-2,6-Diamino-N-((S)-5-amino-6-oxo-6-((4-((perfluoropyridin-4-yl)ethynyl)phenyl)amino)hexyl) hexanamide Trifluoroacetic Acid Salt (3).** Boc-protected compound 11 (100 mg, 0.08 mmol) was dissolved in CH<sub>2</sub>Cl<sub>2</sub> (2 mL) and cooled to 0 °C, followed by addition of trifluoroacetic acid (2 mL). Reaction mixture was stirred for 4 h and was poured in a centrifuge tube containing anhydrous diethyl ether (15 mL). Immediately solid came out, and it was centrifuged. The solid material was washed with anhydrous diethyl ether (2 × 15 mL) to get pure TFA-salt 3 (95 mg, 90%) as white solid. <sup>1</sup>H NMR (400 MHz, CD<sub>3</sub>OD): δ 7.78 (d, J = 8.6 Hz, 2H), 7.64 (d, J = 8.6 Hz, 2H), 4.04 (t, J = 6.6 Hz, 1H), 3.82 (t, J = 6.6 Hz, 1H), 3.29–3.17 (m, 2H), 2.92 (t, J = 7.8 Hz, 2H), 2.06–1.76 (m, 4H), 1.73–1.57 (m, 4H), 1.56–1.39 (m, 4H). <sup>13</sup>C NMR (100 MHz, CD<sub>3</sub>OD): δ 170.2, 169.1, 163.4, 163.0, 144.8 (dm, J = 245 Hz), 143.3 (dm, J = 264 Hz), 141.6, 134.3, 121.1, 117.4, 118.4, 107.3, 74.0, 55.2, 54.3, 40.3, 40.2, 32.3, 32.1, 29.9, 28.1, 23.3, 23.0. MS (ESI): m/z (%) 523 (100) [M + H]<sup>+</sup>. HRMS (ESI): calcd for C<sub>25</sub>H<sub>31</sub>F<sub>4</sub>N<sub>6</sub>O<sub>2</sub> [M + H]<sup>+</sup> 523.24446, found 523.24481.

**tert-Butyl N-[(1S)-5-[(2S)-2,6-Bis(tert-butoxycarbonylamino)hexanoyl]amino]-1-[3,4-bis[2-(2,3,5,6-tetrafluoro-4-pyridyl)ethynyl]phenyl]carbamoyl]pentyl]carbamate (12).** The peptide conjugate 12 was prepared by using the same procedure as synthesis of compound 11 in 60% yield. <sup>1</sup>H NMR (400 MHz, CDCl<sub>3</sub>): δ 9.54 (bs, 1H), 8.06 (d, J = 8.5 Hz, 1H), 7.73 (bs, 1H), 7.61 (d, J = 8.5 Hz, 1H), 6.69 (bs, 1H), 5.78–5.14 (bs, 2H), 4.69 (bs, 1H), 4.33–4.17 (m, 1H), 3.40–2.97 (m, 4H), 2.00–1.19 (m, 39H). <sup>13</sup>C NMR (100 MHz, CDCl<sub>3</sub>): δ 175.4, 174.3, 158.7, 158.2, 157.9, 146.2, 146.1, 143.7, 142.5, 135.2, 125.5, 124.5, 122.9, 119.5, 104.6, 103.9, 80.9, 80.7, 79.9, 57.0, 56.3, 41.1, 40.1, 33.2, 32.9, 30.6, 30.1, 28.9, 28.8, 27.1, 26.7, 24.3. MS (ESI): m/z (%) 1018 (100) [M + Na]<sup>+</sup>. HRMS (ESI): calcd for C<sub>47</sub>H<sub>53</sub>F<sub>8</sub>N<sub>7</sub>O<sub>8</sub>Na [M + Na]<sup>+</sup> 1018.37256, found 1018.37340.

**(S)-2,6-Diamino-N-((S)-5-amino-6-((3,4-bis((perfluoropyridin-4-yl)ethynyl)phenyl)amino)-6-oxohexyl)hexanamide Trifluoroacetic Acid Salt (4).** The Boc-protected compound 4 was prepared by using the same procedure as synthesis of compound 3 in 85% yield. <sup>1</sup>H NMR (600 MHz, CD<sub>3</sub>OD): δ 8.21 (s, 1H), 7.86–7.76 (m, 2H), 4.10–4.03 (m, 1H), 3.78–3.68 (m, 1H), 3.25–3.15 (m, 1H), 2.98–2.89 (m, 2H), 2.09–1.77 (m, 4H), 1.76–1.41 (m, 8H). <sup>13</sup>C NMR (100 MHz, CD<sub>3</sub>OD): δ 170.2, 169.5, 163.5, 163.3, 162.9, 159.4, 145.7, 144.2, 142.5, 141.8, 135.3, 125.7, 124.6, 123.1, 120.2, 117.7, 104.3, 103.8, 78.6, 78.3, 55.3, 54.4, 52.7,

40.4, 40.3, 32.3, 30.6, 28.2, 28.1, 26.4, 22.6. MS (ESI): m/z (%) 696 (100) [M + H]<sup>+</sup>. HRMS (ESI): calcd for C<sub>32</sub>H<sub>30</sub>F<sub>8</sub>N<sub>7</sub>O<sub>2</sub> [M + H]<sup>+</sup> 696.23332, found 696.23180.

**tert-Butyl N-[(5S)-5-[(2S)-2,6-Bis(tert-butoxycarbonylamino)hexanoyl]amino]-6-oxo-6-[4-[2-(2,3,5,6-tetrafluoro-4-pyridyl)ethynyl]anilino]hexyl]carbamate (13).**

The peptide conjugate 13 was prepared by using the same procedure as synthesis of compound 11 in 68% yield. <sup>1</sup>H NMR (400 MHz, CDCl<sub>3</sub>): δ 9.13 (bs, 1H), 7.81–7.73 (m, 2H), 7.54 (d, J = 8.7 Hz, 1H), 6.72 (bs, 1H), 5.80 (bs, 1H), 4.84–4.67 (m, 2H), 4.62–4.52 (m, 1H), 4.12–3.99 (m, 1H), 3.19–3.02 (m, 4H), 2.12–1.64 (m, 5H), 1.63–1.33 (m, 34H). <sup>13</sup>C NMR (100 MHz, CDCl<sub>3</sub>): δ 173.1, 170.4, 156.7, 156.6, 156.2, 144.6, 144.4 (dm, J = 245 Hz), 141.6 (dm, J = 270 Hz), 140.5, 133.2, 119.7, 117.6, 115.5, 107.1, 80.6, 79.3, 73.2, 55.5, 53.9, 40.0, 39.2, 31.4, 30.9, 29.5, 28.5, 28.4, 28.3, 22.8, 22.3. MS (ESI): m/z (%) 845 (100) [M + Na]<sup>+</sup>. HRMS (ESI TOF): calcd for C<sub>40</sub>H<sub>34</sub>F<sub>4</sub>N<sub>6</sub>O<sub>8</sub>Na [M + Na]<sup>+</sup> 845.38369, found 845.38472.

**(S)-2,6-Diamino-N-((S)-6-amino-1-oxo-1-((4-((perfluoropyridin-4-yl)ethynyl)phenyl)amino)hexan-2-yl)hexanamide Trifluoroacetic Acid Salt (5).** The Boc-protected compound 5 was prepared by using the same procedure as synthesis of compound 3 in 95% yield. <sup>1</sup>H NMR (600 MHz, CD<sub>3</sub>OD): δ 7.71 (d, J = 8.7 Hz, 2H), 7.59 (d, J = 8.7 Hz, 2H), 4.51 (dd, J = 8.6, 5.2 Hz, 1H), 3.99 (t, J = 6.4 Hz, 1H), 2.92 (m, 4H), 1.98–1.42 (m, 12H). <sup>13</sup>C NMR (100 MHz, CD<sub>3</sub>OD): δ 172.6, 170.4, 163.4, 163.2, 144.9 (dm, J = 251 Hz), 143.3 (dm, J = 279 Hz), 142.1, 134.3, 121.2, 118.5, 117.1, 107.5, 74.0, 55.9, 54.1, 40.6, 40.4, 32.7, 32.1, 28.4, 28.1, 24.1, 22.6. MS (ESI): m/z (%) 523 (100) [M + H]<sup>+</sup>. HRMS (ESI): calcd for C<sub>25</sub>H<sub>31</sub>F<sub>4</sub>N<sub>6</sub>O<sub>2</sub> [M + H]<sup>+</sup> 523.24446, found 523.24465.

**tert-Butyl N-[(5S)-5-[(2S)-2,6-Bis(tert-butoxycarbonylamino)hexanoyl]amino]-6-[3,4-bis[2-(2,3,5,6-tetrafluoro-4-pyridyl)ethynyl]anilino]-6-oxo-hexyl]carbamate (14).** The peptide conjugate 14 was prepared by using the same procedure as synthesis of compound 11 in 62% yield. <sup>1</sup>H NMR (400 MHz, CDCl<sub>3</sub>): δ 9.29 (bs, 1H), 8.16 (bs, 1H), 8.09–7.97 (m, 1H), 7.64 (d, J = 8.7 Hz, 1H), 6.59 (bs, 1H), 5.95 (bs, 1H), 4.84–4.50 (m, 3H), 4.08–4.01 (m, 1H), 3.23–3.03 (m, 4H), 1.96–1.31 (m, 39H). MS (ESI): m/z (%) 1018 (100) [M + Na]<sup>+</sup>. HRMS (ESI TOF): calcd for C<sub>47</sub>H<sub>53</sub>F<sub>8</sub>N<sub>7</sub>O<sub>8</sub>Na [M + Na]<sup>+</sup> 1018.37256, found 1018.37108.

**(S)-2,6-Diamino-N-((S)-6-amino-1-((3,4-bis((perfluoropyridin-4-yl)ethynyl)phenyl)amino)-1-oxohexan-2-yl)hexanamide Trifluoroacetic Acid Salt (6).** The Boc-protected compound 6 was prepared by using the same procedure as synthesis of compound 3 in 86% yield. <sup>1</sup>H NMR (400 MHz, CD<sub>3</sub>OD): δ 8.14 (d, J = 1.8 Hz, 1H), 7.79 (dd, J = 8.6, 1.8 Hz, 1H), 7.73 (d, J = 8.6 Hz, 1H), 4.54 (d, J = 8.7, 5.1 Hz, 1H), 3.99 (t, J = 6.3 Hz, 1H), 2.99–2.91 (m, 4H), 2.03–1.79 (m, 4H), 1.79–1.60 (m, 4H), 1.66–1.45 (m, 4H). <sup>13</sup>C NMR (150 MHz, CD<sub>3</sub>OD): δ 172.8, 169.1, 163.1, 145.7, 144.1, 142.6, 142.3, 135.2, 125.6, 124.4, 122.9, 119.8, 104.3, 103.8, 78.5, 78.2, 55.9, 54.1, 40.5, 40.4, 32.6, 32.4, 28.4, 28.2, 24.1, 22.8. MS (ESI): m/z (%) 696 (100) [M + H]<sup>+</sup>. HRMS (ESI): calcd for C<sub>32</sub>H<sub>30</sub>F<sub>8</sub>N<sub>7</sub>O<sub>2</sub> [M + H]<sup>+</sup> 696.23332, found 696.23180.

**Plasmid DNA Photocleavage.** pBR322 plasmid DNA (4361 bp; from BioLabs Inc., 1 μg/μL solution in 10 mM Tris-HCl (pH 8.0), and 1 mM EDTA buffer) was diluted to a concentration of 0.01 μg/μL. The solution containing cleavage agent, DNA (38 μM/bp) in 20 mM sodium phosphate buffer was incubated for 1 h at 30 °C. Samples were placed on ice at a distance of 20 cm from 200 W Hg–Xe lamp (Spectra-Physics, Laser & Photonics Oriel Instruments with long pass filter with 324 nm cut-on wavelength).

**Electrophoretic Analysis.** The gel electrophoresis was carried out in 1× TBE buffer at 80 V using Miligel FisherBiotech horizontal electrophoresis system. All gels were run on 1% agarose slab gels. Before loading, the DNA samples were mixed with 0.33 volume of tracking dye containing bromophenol blue (0.25%) and glycerol (30%) in water. After staining in ethidium bromide solution (2 μg/mL) for 1 h, the gel was washed with water and pictures were taken. The relative quantities of the supercoiled and nicked, and linear DNA were calculated by integrating the “area” of each spot by the image analyzer software Total/Lab (Nonlinear Dynamics Ltd., UK). The amount of supercoiled DNA was multiplied by a factor of 1.4 to

account for reduced ethidium bromide intercalation into supercoiled DNA.

**Spectrometric Determinations of  $pK_a$ .** pH of 10  $\mu\text{M}$  of compound solution in  $\text{H}_2\text{O}$  was adjusted with 10, 100 mM HCl (aq) and NaOH (aq) solution under nitrogen purged condition. Excitation wavelength was 330 nm and polymethacrylate fluorimeter cuvettes were used.

**Alkaline Single-Cell Gel Electrophoresis Assay.** LMAgarose was melt in boiling water bath for 5 min and placed in 37 °C water bath for at least 20 min to cool. Cells at  $2 \times 10^5/\text{mL}$  were combined with molten LMAgarose at a ratio of 1: 10 (v/v) and 50  $\mu\text{L}$  of the mixture was transferred on CometSlides and lysed overnight at 4 °C. After that, the slides were immersed in alkaline solution prepared freshly with NaOH (0.6 g), 200 mM EDTA (250  $\mu\text{L}$ ), and  $\text{dH}_2\text{O}$  (49.75 mL) for 20 min at room temperature, in the dark. Then, the slides were removed from alkaline solution and washed by immersing in 1 $\times$  TBE buffer for 5 min twice. After adding alkaline electrophoresis buffer 1 mm above slides, the voltage at 1 V per cm was applied and the volume of buffer adjusted to reach 300 mA. Electrophoresis was run at 4 °C for 30 min. The samples were dried at  $\leq 45$  °C for 15 min, and 100  $\mu\text{L}$  of diluted SYBR Green I was placed on the gels and the slides were stored at refrigerator. After 5 min, excess SYBR solution was removed by gentle tapping, and the slides were completely dried at room temperature in the dark. The fluorescence images were taken by epifluorescence microscopy.

**Cell Culture.** The human malignant melanoma cell line A375 (CRL-1619) was obtained from the American Type Culture Collection (ATCC). The cell line were cultured in RPMI 1640 medium supplemented with 10% fetal bovine serum (FBS) and penicillin/streptomycin (Life Technologies). Cells were propagated according to ATCC guidelines and maintained in a 37 °C incubator with 5%  $\text{CO}_2$  atmosphere.

**MTT Assay.** Half-maximal Inhibitory concentrations ( $\text{CC}_{50}$ ) for the compounds tested were determined using the metabolic assay MTT (dimethyl thiazolyl diphenyl tetrazolium salt) that measures conversion of MTT into formazan by the mitochondrial reductase producing a purple color. A375 cell lines were seeded at 2500 cells per well in a 96-well plate. Seven 2-fold serial dilutions of the compounds were added to the cells in triplicate. After 4 h of incubation with the compounds, cells were UV-irradiated for 10 min at 365 nm (UV transilluminator, Spectronics Corp. model TR-365R). After 72 h, MTT (Sigma cat. no. M2128) was added to cells to a final concentration of 1.25 mg/mL. After 60 min cells were centrifuged at 900g for 5 min at room temperature. Media was replaced with DMSO, and absorbance was measured in a multidetection microplate reader Synergy HT, from BIOTEK at 600 nm. Graphical representation was generated using the software Prism version 4 from GraphPad.

**DNA Fragmentation Assay.** A375 cells ( $5 \times 10^5$ ) were plated in 10 cm cell culture dishes. Twenty-four hours later, 30  $\mu\text{M}$  of KK (1a,2e)-Ac (5) was added to cells and incubated for 3 h. Treated and untreated cells were exposed to UV radiation for 20 min and harvested at 6, 24, and 48 h post UV radiation. DNA from harvested cells was extracted using GeneElute Mammalian Genomic DNA kit (cat. no. G1N70, Sigma-Aldrich, Co). DNA was electrophoresed on a 1.6% agarose-TAE gel.

## ■ ASSOCIATED CONTENT

### ■ Supporting Information

Fluorescence data, diagrams for plasmid relaxation assay,  $^1\text{H}$  and  $^{13}\text{C}$  NMR spectroscopic data for new compounds. This material is available free of charge via the Internet at <http://pubs.acs.org>.

## ■ AUTHOR INFORMATION

### Corresponding Author

\*Phone: 1-850-644-5795. E-mail: [alabugin@chem.fsu.edu](mailto:alabugin@chem.fsu.edu).

## ■ ACKNOWLEDGMENTS

I.A. is grateful to the National Science Foundation (CHE-0848686) and James & Esther King Biomedical Research Program (09KC-03) for support of this research project.

## ■ ABBREVIATIONS USED

ss, single-stranded; ds, double-stranded; TPA, two-photon absorption; OG, 8-oxo-guanine; TFA, trifluoroacetic acid; DIC, differential interference contrast; SCGE, single-cell gel electrophoresis

## ■ REFERENCES

- (1) Choi, H. S.; Huh, K. M.; Ooya, T.; Yui, N. pH- and Thermosensitive Supramolecular Assembling System: Rapidly Responsive Properties of  $\beta$ -Cyclodextrin-Conjugated Poly( $\epsilon$ -lysine). *J. Am. Chem. Soc.* **2003**, *125*, 6350–6351.
- (2) Fabbri, L.; Gatti, F.; Pallavicini, P.; Parodi, L. An 'off-on-off' fluorescent sensor for pH based on ligand-proton and ligand-metal-proton interactions. *New J. Chem.* **1998**, *22*, 1403–1407.
- (3) de Silva, A. P.; Gunaratne, H. Q. N.; McCoy, C. P. Direct visual indication of pH windows: 'off-on-off' fluorescent PET (photoinduced electron transfer) sensors/switches. *Chem. Commun.* **1996**, 2399–2400.
- (4) Saha, S.; Stoddart, J. F. Photo-driven molecular devices. *Chem. Soc. Rev.* **2007**, *36*, 77–92.
- (5) Silvi, S.; Arduini, A.; Pochini, A.; Secchi, A.; Tomasulo, M.; Raymo, F. M.; Baroncini, M.; Credi, A. A Simple Molecular Machine Operated by Photoinduced Proton Transfer. *J. Am. Chem. Soc.* **2007**, *129*, 13378–13379.
- (6) Xue, C.; Mirkin, C. A. pH-Switchable Silver Nanoprism Growth Pathways. *Angew. Chem., Int. Ed.* **2007**, *46*, 2036–2038.
- (7) Schnarr, N. A.; Kennan, A. pH-Switchable Strand Orientation in Peptide Assemblies. *Org. Lett.* **2005**, *7*, 395–398. Schnarr, N. A.; Kennan, A. J. pH-Triggered Strand Exchange in Coiled-Coil Heterotrimers. *J. Am. Chem. Soc.* **2003**, *125*, 6364–6365. Rooth, M.; Shaw, A. M. pH-Controlled Formation Kinetics of Self-Assembled Layers of Thioctic Acid on Gold Nanoparticles. *J. Phys. Chem. C* **2007**, *111*, 15363–15369. Xu, H.; Stamp, S. P.; Rudkevich, D. M. A pH Switch in Supramolecular Polymeric Capsules. *Org. Lett.* **2003**, *5*, 4583–4586. Martínez-Díaz, M.-V.; Spencer, N.; Stoddart, J. F. The Self-Assembly of a Switchable [2]Rotaxane. *Angew. Chem., Int. Ed.* **1997**, *36*, 1904–1907. Ashton, P. R.; Ballardini, R.; Balzani, V.; Baxter, I.; Credi, A.; Fyfe, M. C. T.; Gandolfi, M. T.; Gomez-Lopez, M.; Martínez-Díaz, M.-V.; Piersanti, A.; Spencer, N.; Stoddart, J. F.; Venturi, M.; White, A. J. P.; Williams, D. J. Acid-Base Controllable Molecular Shuttles. *J. Am. Chem. Soc.* **1998**, *120*, 11932–11942. Elizarov, A. M.; Chang, T.; Chiu, H.-S.; Stoddart, J. F. An Acid-Base Switchable [2]Rotaxane. *J. Org. Chem.* **2002**, *67*, 9175–9181. Leigh, D. A.; Thomson, A. R. Switchable Dual Binding Mode Molecular Shuttle. *Org. Lett.* **2006**, *8*, 5377–5379. Becuwe, M.; Cazier, F.; Bria, M.; Woisel, P.; Delattre, F. Tuneable fluorescent marker appended to  $\beta$ -cyclodextrin: a pH-driven molecular switch. *Tetrahedron Lett.* **2007**, *48*, 6186–6188. Pallavicini, P.; Amendola, V.; Massera, C.; Mundum, E.; Taglietti, A. 'On-off-on' fluorescent indicators of pH windows based on three separated components. *Chem. Commun.* **2002**, 2452–2453. Gunnlaugsson, T.; Leonard, J. P.; Senechal, K.; Harte, A. J. pH Responsive Eu(III)-Phenanthroline Supramolecular Conjugate: Novel 'Off-On-Off' Luminescent Signaling in the Physiological pH Range. *J. Am. Chem. Soc.* **2003**, *125*, 12062–12063. Tajc, S. G.; Miller, B. L. A Designed Receptor for pH-Switchable Ion Binding in Water. *J. Am. Chem. Soc.* **2006**, *128*, 2532–2533. Fattakhova-Rohlfing, D.; Wark, M.; Rathousky, J. Ion-Permeable pH-Switchable Mesoporous Silica Thin Layers. *Chem. Mater.* **2007**, *19*, 1640–1647. Turega, S. M.; Philp, D. Controlling a recognition-mediated reaction using a pH switch. *Chem. Commun.* **2006**, *35*, 3684–3686. Broz, P.; Driamov, S.; Ziegler, J.; Ben-Haim, N.; Marsch, S.; Meier, W.; Hunziker, P. Toward Intelligent Nanosize Bioreactors: A pH-Switchable, Channel-

Equipped, Functional Polymer Nanocontainer. *Nano Lett.* **2006**, *6*, 2349–2363.

(8) Gabr, A.; Kuin, A.; Aalders, M.; El-Gawly, H.; Smets, L. A. Cellular Pharmacokinetics and Cytotoxicity of Camptothecin and Topotecan at Normal and Acidic pH. *Cancer Res.* **1997**, *57*, 4811–4816. Adams, D. J.; Dewhirst, M. W.; Flowers, J. L.; Gamcsik, M. P.; Colvin, O. M.; Manikumar, G.; Wani, M. C.; Wall, M. E. Camptothecin analogues with enhanced antitumor activity in acidic pH. *Cancer Chemother. Pharmacol.* **2000**, *46*, 263–271. Wachsberger, P. R.; Burd, R.; Wahl, M. L.; Leeper, D. B. Betulinic acid sensitization of low pH adapted human melanoma cells to hyperthermia. *Int. J. Hyperthermia* **2002**, *18*, 153–164.

(9) Wood, P. J.; Sansom, J. M.; Newell, K.; Tannock, I. F.; Stratford, I. J. Reduction of tumour intracellular pH and enhancement of melphalan cytotoxicity by the ionophore nigericin. *Int. J. Cancer* **1995**, *60*, 264–268. Vukovic, V.; Tannock, I. F. Influence of low pH on cytotoxicity of paclitaxel, mitoxantrone and topotecan. *Br. J. Cancer* **1997**, *75*, 1167–1172.

(10) Hoffner, J.; Schottelius, J.; Feichtinger, D.; Chen, P. Chemistry of the 2,5-didehydropyridine biradical: computational, kinetic, and trapping studies toward drug design. *J. Am. Chem. Soc.* **1998**, *120*, 376–385.

(11) Priyadarsini, K. I.; Dennis, M. F.; Naylor, M. A.; Stratford, M. R. L.; Wardman, P. Free Radical Intermediates in the Reduction of Quinoxaline N-Oxide Antitumor Drugs: Redox and Prototropic Reactions. *J. Am. Chem. Soc.* **1996**, *118*, 5648–5654, and references therein.

(12) Stubbs, M.; Rodrigues, L.; Howe, F. A.; Wang, J.; Jeong, K. S.; Veech, R. L.; Griffiths, J. R. Metabolic Consequences of a Reversed pH Gradient in Rat Tumors. *Cancer Res.* **1994**, *54*, 4011–4016.

(13) Song, C. W.; Lyons, J. C.; Griffin, R. J.; Makepeace, C. M. Thermosensitization by lowering intracellular pH with 5-(N-ethyl-N-isopropyl) amiloride. *Radiother. Oncol.* **1993**, *27*, 252–258. Lyons, J. C.; Song, C. Killing of Hypoxic Cells by Lowering the Intracellular pH in Combination with Hyperthermia. *Radiat. Res.* **1995**, *141*, 216–218.

(14) Newell, K.; Wood, P.; Stratford, I.; Tannock, I. Effects of agents which inhibit the regulation of intracellular pH on murine solid tumours. *Br. J. Cancer* **1992**, *66*, 311–317. Osinsky, S. P.; Bubnovskaya, L. N.; Sergienko, T. Tumour pH under induced hyperglycemia and efficacy of chemotherapy. *Anticancer Res.* **1987**, *7*, 199–201.

(15) Tannock, I. F.; Rotin, D. Acid pH in Tumors and Its Potential for Therapeutic Exploitation. *Cancer Res.* **1989**, *49*, 4373–4384.

(16) Wike-Hooley, J. L.; Haveman, J.; Reinhold, H. S. The relevance of tumour pH to the treatment of malignant disease. *Radiother Oncol.* **1984**, *2*, 343–366.

(17) Kar, M.; Basak, A. Design, Synthesis, and Biological Activity of Unnatural Eneidyne and Related Analogues Equipped with pH-Dependent or Phototriggering Devices. *Chem. Rev.* **2007**, *107*, 2861–2890.

(18) Stanulla, M.; Wang, J.; Chervinsky, D. S.; Thandla, S.; Aplan, P. D. DNA cleavage within the MLL breakpoint cluster region is a specific event which occurs as part of higher-order chromatin fragmentation during the initial stages of apoptosis. *Mol. Cell. Biol.* **1997**, *17*, 4070–4079.

(19) Galm, U.; Hager, M. H.; Van Lanen, S. G.; Ju, J.; Thorson, J. S.; Shen, B. Antitumor Antibiotics: Bleomycin, Eneidyne, and Mitomycin. *Chem. Rev.* **2005**, *105*, 739–758.

(20) Elmroth, K.; Nygren, J.; Martensson, S.; Ismail, I. H.; Hammarsten, O. Cleavage of Cellular DNA by Calicheamicin  $\gamma$ 1. *DNA Repair* **2003**, *2*, 363–374.

(21) Watson, J. D.; Baker, T. A.; Bell, S. P.; Gann, A.; Levine, M.; Losick, R., Eds. *Molecular Biology of the Gene*, 5th ed.; Cold Spring Harbor Laboratory Press: Plainview, NY, 2004; Chapters 9 and 10.

(22) Armitage, B. Photocleavage of Nucleic Acids. *Chem. Rev.* **1998**, *98*, 1171–1200. and references therein. Jones, G. B.; Wright, J. M.; Plourde, G. II; Purohit, A. D.; Wyatt, J. K.; Hynd, G.; Fouad, F. Synthesis and Photochemical Activity of Designed Eneidyne. *J. Am. Chem. Soc.* **2000**, *122*, 9872–9873. Kagan, J.; Wang, X.; Chen, X.; Lau,

K. Y.; Batac, I. V.; Tuveson, R. W.; Hudson, J. B. DNA Cleavage, antiviral and cytotoxic reactions photosensitized by simple enediyne compounds. *J. Photochem. Photobiol., B* **1993**, *21*, 135–142. Benites, P. J.; Holmberg, R. C.; Rawat, D. S.; Kraft, B. J.; Klein, L. J.; Peters, D. G.; Thorp, H. H.; Zaleski, J. M. Metal–Ligand Charge-Transfer-Promoted Photoelectronic Bergman Cyclization of Copper Metalloenediynes: Photochemical DNA Cleavage via C-4 H-Atom Abstraction. *J. Am. Chem. Soc.* **2003**, *125*, 6434–6446. Poloukhine, A.; Karpov, G.; Popik, V. V. Towards Photoswitchable Eneidyne Antibiotics: Single and Two-Photon Triggering of Bergman Cyclization. *Curr. Top. Med. Chem.* **2008**, *8*, 460–469. Tachi, Y.; Dai, W.-M.; Tanabe, K.; Nishimoto, S.-I. Synthesis and DNA cleavage reaction characteristics of enediyne prodrugs activated via an allylic rearrangement by base or UV irradiation. *Bioorg. Med. Chem.* **2006**, *14*, 3199–3209. Bhattacharyya, S.; Zaleski, J. M. Metalloenediynes: Advances in the Design of Thermally and Photochemically Activated Diradical Formation for Biomedical Applications. *Curr. Top. Med. Chem.* **2004**, *4*, 1637–1654. Schmittel, M.; Viola, G.; Dall'Acqua, F.; Morbach, G. A novel concept to activate enediynes for DNA cleavage. *Chem. Commun.* **2003**, *5*, 646–647. Karpov, G.; Kuzmin, A.; Popik, V. V. Enhancement of the Reactivity of Photochemically Generated Eneidyne via Keto–Enol Tautomerization. *J. Am. Chem. Soc.* **2008**, *130*, 11771–11777. Sud, D.; Wigglesworth, T. J.; Branda, N. R. Creating a Reactive Eneidyne by Using Visible Light: Photocontrol of the Bergman Cyclization. *Angew. Chem., Int. Ed.* **2007**, *46*, 8017–8019. Karpov, G. V.; Popik, V. V. Triggering of the Bergman Cyclization by Photochemical Ring Contraction. Facile Cycloaromatization of Benzannulated Cyclodeca-3,7-diene-1,5-diynes. *J. Am. Chem. Soc.* **2007**, *129*, 3792–3793. Poloukhine, A.; Popik, V. V. Two-Photon Photochemical Generation of Reactive Eneidyne. *J. Org. Chem.* **2006**, *71*, 7417–7421. O'Connor, J. M.; Friese, S. J.; Rodgers, B. L. A Transition-Metal-Catalyzed Eneidyne Cycloaromatization. *J. Am. Chem. Soc.* **2005**, *127*, 16342–16343. Kar, M.; Basak, A.; Bhattacharjee, M. Photoisomerization as a trigger for Bergman cyclization: synthesis and reactivity of azoenediynes. *Bioorg. Med. Chem. Lett.* **2005**, *15*, 5392–5396. Zhao, Z.; Peacock, J. G.; Gubler, D. A.; Peterson, M. A. Photoinduced Bergman cycloaromatization of imidazole-fused enediynes. *Tetrahedron Lett.* **2005**, *46*, 1373–1375. Fouad, F. S.; Crasto, C. F.; Lin, Y.; Jones, G. B. Photoactivated enediynes: targeted chimeras which undergo photo-Bergman cyclization. *Tetrahedron Lett.* **2004**, *45*, 7753–7756. Jones, G. B.; Russell, K. C. *CRC Handbook of Organic Photochemistry and Photobiology*, 2nd ed.; CRC-Press: New York, 2004, 29/1–29/21. Chandra, T.; Kraft, B. J.; Huffman, J. C.; Zaleski, J. M. Synthesis and Structural Characterization of Porphyrinic Eneidyne: Geometric and Electronic Effects on Thermal and Photochemical Reactivity. *Inorg. Chem.* **2003**, *42*, 5158–5172. Banfi, L.; Guanti, G.; Rasparini, M. Intramolecular Opening of  $\beta$ -Lactams with Amines as a Strategy Toward Enzymatically or Photochemically Triggered Activation of Lactenediyne Prodrugs. *Eur. J. Org. Chem.* **2003**, 1319–1336. Kaneko, T.; Takahashi, M.; Hiram, M. Photochemical Cycloaromatization of Non-Benzenoid Eneidyne. *Angew. Chem., Int. Ed.* **1999**, *38*, 1267–1268. Evenzahav, A.; Turro, N. J. Photochemical Rearrangement of Eneidyne: Is a “Photo-Bergman” Cyclization a Possibility? *J. Am. Chem. Soc.* **1998**, *120*, 1835–1841. Nicolaou, V. K. C.; Dai, W. M.; Wendeborn, S. V.; Smith, A. L.; Torisawa, Y.; Maligres, P.; Hwang, C. K. Eneidyne Compounds with Acid-, Base- and Photo-Sensitive Trigger Groups. Chemical Simulation of the Dynemicin A Reaction Cascade. *Angew. Chem.* **1991**, *103*, 1034–1038. Falcone, D.; Li, J.; Kale, A.; Jones, G. B. Photoactivated enediynes as targeted antitumoral agents: efficient routes to antibody and gold nanoparticle conjugates. *Bioorg. Med. Chem. Lett.* **2008**, *18*, 934–937. Fouad, F. S.; Wright, J. M.; Plourde, G. II; Purohit, A. D.; Wyatt, J. K.; El-Shafey, A.; Hynd, G.; Crasto, C. F.; Lin, Y.; Jones, G. B. Synthesis and Protein Degradation Capacity of Photoactivated Eneidyne. *J. Org. Chem.* **2005**, *70*, 9789–9797. Kraft, B. J.; Coalter, N. L.; Nath, M.; Clark, A. E.; Siedle, A. R.; Huffman, J. C.; Zaleski, J. M. Photothermally Induced Bergman Cyclization of Metalloenediynes via Near-Infrared Ligand-to-Metal Charge-Transfer Excitation. *Inorg. Chem.* **2003**, *42*, 1663–1672.

Plourde, G.; El-Shafey, A.; Fouad, F. S.; Purohit, A. S.; Jones, G. B. Protein degradation with photoactivated enediyne-amino acid conjugates. *Bioorg. Med. Chem. Lett.* **2002**, *12*, 2985–2988. Basak, A.; Bdour, H. M.; Shain, J. C.; Mandal, S.; Rudra, K. R.; Nag, S. DNA-Cleavage studies on *N*-substituted monocyclic enediynes: enhancement of potency by incorporation of intercalating or electron poor aromatic ring and subsequent design of a novel phototriggerable acyclic enediyne. *Bioorg. Med. Chem. Lett.* **2000**, *10*, 1321–1325.

(23) Kovalenko, S. V.; Alabugin, I. V. Lysine–enediyne conjugates as photochemically triggered DNA double-strand cleavage agents. *Chem. Commun.* **2005**, 1444–1446.

(24) Yang, W.-Y.; Breiner, B.; Kovalenko, S. V.; Ben, C.; Singh, M.; LeGrand, S. N.; Sang, Q.-X. A.; Strouse, G. F.; Copland, J. A.; Alabugin, I. V. C-Lysine Conjugates: pH-Controlled Light-Activated Reagents for Efficient Double-Stranded DNA Cleave with Implications for Cancer Therapy. *J. Am. Chem. Soc.* **2009**, *131*, 11458–11470.

(25) Breiner, B.; Schlatterer, J. C.; Kovalenko, S. V.; Greenbaum, N. L.; Alabugin, I. V. Protected <sup>32</sup>P-labels in Deoxyribonucleotides: Investigation of Sequence Selectivity of DNA Photocleavage by Enediyne-, Fulvene-, and Acetylene-lysine Conjugates. *Angew. Chem., Int. Ed.* **2007**, *45*, 3666–3670.

(26) Breiner, B.; Schlatterer, J. C.; Kovalenko, S. V.; Greenbaum, N. L.; Alabugin, I. V. DNA Damage-Site Recognition by Lysine Conjugates. *Proc. Natl. Acad. Sci. U.S.A.* **2007**, *104*, 13016–13021.

(27) Yang, W.-Y.; Cao, Q.; Callahan, C.; Galvis, C.; Sang, A. Q.-X.; Alabugin, I. V. Intracellular DNA damage by lysine-acetylene conjugates. *J. Nucleic Acids* **2010**, Article ID 931394.

(28) Kauffman, J. F.; Turner, J. M.; Alabugin, I. V.; Breiner, B.; Kovalenko, S. V.; Badaeva, E. A.; Masunov, A.; Tretiak, S. Two-Photon Excitation of Substituted Eneidyne. *J. Phys. Chem. A* **2006**, *110*, 241–251.

(29) Saito, I.; Takayama, M.; Sugiyama, H.; Nakatani, H. Photoinduced DNA Cleavage via Electron Transfer: Demonstration That Guanine Residues Located 5' to Guanine Are the Most Electron-Donating Sites. *J. Am. Chem. Soc.* **1995**, *117*, 6406–6407. Saito, I.; Takayama, M.; Kawanishi, S. Photoactivatable DNA-Cleaving Amino Acids: Highly Sequence-Selective DNA Photocleavage by Novel L-Lysine Derivatives. *J. Am. Chem. Soc.* **1995**, *117*, 5590–5591. Plourde, G. II; El-Shafey, A.; Fouad, F. S.; Purohit, A. S.; Jones, G. B. Protein degradation with photoactivated enediyne-amino acid conjugates. *Bioorg. Med. Chem. Lett.* **2002**, *12*, 2985–2988. Rao, M. V.; Menon, S. K. Photoinduced DNA cleavage by fullerene–lysine conjugate. *Tetrahedron Lett.* **2009**, *50*, 6526–6530.

(30) Photochemical or radical cross-linking with amino acids: Sun, G.; Fecko, C. J.; Nicewonger, R. B.; Webb, W. W.; Begley, T. P. DNA–Protein Cross-Linking: Model Systems for Pyrimidine–Aromatic Amino Acid Cross-Linking. *Org. Lett.* **2006**, *8*, 681–683. Margolis, S. A.; Coxon, B.; Gajewski, E.; Dizdaroglu, M. Structure of a hydroxyl radical induced cross-link of thymine and tyrosine. *Biochemistry* **1988**, *27*, 6353–6359. Dizdaroglu, M.; Gajewski, E. Structure and Mechanism of Hydroxyl Radical-induced Formation of a DNA-Protein Cross-Link Involving Thymine and Lysine in Nucleohistone. *Cancer Res.* **1989**, *49*, 3463–3467. Gajewski, E.; Dizdaroglu, M. Hydroxyl radical induced cross-linking of cytosine and tyrosine in nucleohistone. *Biochemistry* **1990**, *29*, 977–980. Morin, B.; Cadet, J. Benzophenone Photosensitization of 2'-Deoxyguanosine: Characterization of the 2R And 2s Diastereoisomers of 1-(2-Deoxy-β-D-erythroW-pentofuranosyl)-2-methoxy-4,5-imidazolidinedione. A Model System For The Investigation Of Photosensitized Formation Of DNA–Protein Crosslinks. *Photochem. Photobiol.* **1994**, *60*, 102–109. Morin, B.; Cadet, J. Chemical Aspects of the Benzophenone-Photosensitized Formation of Two Lysine-2'-deoxyguanosine Cross-Links. *J. Am. Chem. Soc.* **1995**, *117*, 12408–12415. Morin, B.; Cadet, J. Type I Benzophenone-Mediated Nucleophilic Reaction of 5'-Amino-2',5'-dideoxyguanosine. A Model System for the Investigation of Photosensitized Formation of DNA–Protein Cross-Links. *Chem. Res. Toxicol.* **1995**, *8*, 792–799. Cross-links between histones and oxidized DNA: Kurbanyan, K.; Nguyen, K. L.; To, P.; Rivas, E. V.; Lueras, A. M.

K.; Kosinski, C.; Steryo, M.; Gonzalez, A.; Mah, D. A.; Stemp, E. D. A. DNA–Protein Cross-Linking via Guanine Oxidation: Dependence upon Protein and Photosensitizer. *Biochemistry* **2003**, *42*, 10269–10281. Nguyen, K. L.; Steryo, M.; Kurbanyan, K.; Nowitzki, K. M.; Butterfield, S. M.; Ward, S. R.; Stemp, E. D. A. DNA–Protein Cross-Linking from Oxidation of Guanine via the Flash–Quench Technique. *J. Am. Chem. Soc.* **2000**, *122*, 3585–3594. Cross-links between the TGT trinucleotide and KKK tripeptide mediated by photooxidation: Perrier, S.; Hau, J.; Gasparutto, D.; Cadet, J.; Favier, A.; Ravanat, J. L. Characterization of Lysine–Guanine Cross-Links upon One-Electron Oxidation of a Guanine-Containing Oligonucleotide in the Presence of a Trilycine Peptide. *J. Am. Chem. Soc.* **2006**, *128*, 5703–5710.

(31) Hickerson, R. P.; Chepanoske, C. L.; Williams, S. D.; David, S. S.; Burrows, C. J. Mechanism-Based DNA–Protein Cross-Linking of MutY via Oxidation of 8-Oxoguanosine. *J. Am. Chem. Soc.* **1999**, *121*, 9901–9902. Hosford, M. E.; Muller, J. G.; Burrows, C. J. Spermene Participates in Oxidative Damage of Guanosine and 8-Oxoguanosine Leading to Deoxyribosylurea Formation. *J. Am. Chem. Soc.* **2004**, *126*, 9540–9541. Johansen, M. E.; Muller, J. G.; Xu, X.; Burrows, C. J. Oxidatively Induced DNA–Protein Cross-Linking between Single-Stranded Binding Protein and Oligodeoxynucleotides Containing 8-Oxo-7,8-dihydro-2'-deoxyguanosine. *Biochemistry* **2005**, *44*, 5660–5671. Xu, X.; Muller, J. G.; Ye, Y.; Burrows, C. J. DNA–Protein Cross-links between Guanine and Lysine Depend on the Mechanism of Oxidation for Formation of C5 Vs C8 Guanosine Adducts. *J. Am. Chem. Soc.* **2008**, *130*, 703–709.

(32) Hawkins, C. L.; Pattison, D. I.; Davies, M. J. Reaction of protein chloramines with DNA and nucleosides: evidence for the formation of radicals, protein–DNA cross-links and DNA damage mediated by protein chloramines. *Biochem. J.* **2002**, *365*, 605–615. For reactions of other oxidized protein forms with DNA, see also: Prestwich, E. G.; Roy, M. D.; Rego, J.; Kelley, S. O. Oxidative DNA Strand Scission Induced by Peptides. *Chem. Biol.* **2005**, *12*, 695–701.

(33) Szczepanski, J. T.; Wong, R. S.; McKnight, J. N.; Bowman, G. D.; Greenberg, M. M. Rapid DNA–protein cross-linking and strand scission by an abasic site in a nucleosome core particle. *Proc. Natl. Acad. Sci. U.S.A.* **2010**, *107*, 22475–22480. Bruner, S. D.; Norman, D. P. G.; Verdine, G. L. Structural basis for recognition and repair of the endogenous mutagen 8-oxoguanine in DNA. *Nature* **2000**, *403*, 859–866. Dodson, M. L.; Schrock, R. D. III.; Lloyd, R. S. Evidence for an imino intermediate in the T4 endonuclease V reaction. *Biochemistry* **1993**, *32*, 8284–8290. Dodson, M. L.; Michaels, M. L.; Lloyd, R. S. Unified catalytic mechanism for DNA glycosylases. *J. Biol. Chem.* **1994**, *269*, 32709–32712. Faucher, F.; Wallace, S. S.; Doublé, S. The C-terminal Lysine of Ogg2 DNA Glycosylases is a Major Molecular Determinant for Guanine/8-Oxoguanine Distinction. *J. Mol. Biol.* **2010**, *397*, 46–56.

(34) Basicity of these groups is known to be sensitive to the environment. See, for example: Highbarger, L. A.; Gerlt, J. A.; Kenyon, G. L. Mechanism of the Reaction Catalyzed by Acetoacetate Decarboxylase. Importance of Lysine 116 in Determining the pK<sub>a</sub> of Active-Site Lysine 115. *Biochemistry* **1996**, *35*, 41–46.

(35) Gao, G.; DeRose, E. F.; Kirby, T. W.; London, R. E. NMR Determination of Lysine pK<sub>a</sub> Values in the Pol λ Lyase Domain: Mechanistic Implications. *Biochemistry* **2006**, *45*, 1785–1794.

(36) To allow comparison of these pK<sub>a</sub>s with pK<sub>a</sub>s obtained by other methods, one has to take into account the difference between pK<sub>a</sub>H<sup>\*</sup>, which is obtained by a direct reading of the H<sub>2</sub>O-calibrated pH meter in a D<sub>2</sub>O solution, and pK<sub>a</sub> (pK<sub>a</sub> = 0.929pK<sub>a</sub>H<sup>\*</sup> + 0.42). pK<sub>a</sub> values measured with pH<sup>\*</sup> are assumed to be similar to the corresponding values in H<sub>2</sub>O: Primrose, W. U. *NMR of Macromolecules. A Practical Approach*; Roberts, G. C. K., Ed.; Oxford University Press: Oxford, 1993, pp 22–23.

(37) Krezel, A.; Bal, W. A formula for correlating pK<sub>a</sub> values determined in D<sub>2</sub>O and H<sub>2</sub>O. *J. Inorg. Biochem.* **2004**, *98*, 161–166.

(38) Carey, F. A. *Organic Chemistry*, 6th ed.; McGraw Hill: New York, 2006.

(39) Note that higher ratios (up to 1:1.3) have been observed for selected DNA sequences: Keck, M. V.; Manderville, R. A.; Hecht, S.

M. Chemical and Structural Characterization of the Interaction of Bleomycin A<sub>2</sub> with d(CGCGAATTCGCG)<sub>2</sub>. Efficient, Double-Strand DNA Cleavage Accessible without Structural Reorganization. *J. Am. Chem. Soc.* **2001**, *123*, 8690–8700. Giroux, R. A.; Hecht, S. M. Characterization of Bleomycin Cleavage Sites in Strongly Bound Hairpin DNAs. *J. Am. Chem. Soc.* **2010**, *132*, 16987–16996.

(40) Tounekti, O.; Kenani, A.; Foray, N.; Orłowski, S.; Mir, L. M. The ratio of single- to double-strand DNA breaks and their absolute values determine cell death pathway. *Brit. J. Cancer.* **2001**, *84*, 1272–1279.

(41) Povirk, L. F.; Han, Y. H.; Steighner, R. J. Structure of bleomycin-induced DNA double-strand breaks: predominance of blunt ends and single-base 5' extensions. *Biochemistry* **1989**, *28*, 5808–5814.

(42) Absalon, M. J.; Kozarich, J. W.; Stubbe, J. Sequence Specific Double-Strand Cleavage of DNA by Fe-Bleomycin. 1. The Detection of Sequence-Specific Double-Strand Breaks Using Hairpin Oligonucleotides. *Biochemistry* **1995**, *34*, 2065–2075. Stubbe, J.; Kozarich, J. W.; Wu, W.; Vanderwall, D. E. Bleomycins: A Structural Model for Specificity, Binding, and Double Strand Cleavage. *Acc. Chem. Res.* **1996**, *29*, 322–330.

(43) Charles, K.; Povirk, L. F. Action of Bleomycin on Structural Mimics of Intermediates in DNA Double-Strand Cleavage. *Chem. Res. Toxicol.* **1998**, *11*, 1580–1585.

(44) Grimwade, J. E.; Beerman, T. A. Measurement of Bleomycin, Neocarzinostatin, and Auromomycin Cleavage of Cell-Free and Intracellular Simian Virus 40 DNA and Chromatin. *Mol. Pharmacol.* **1986**, *30*, 358–363.

(45) Povirk, L. F.; Wübker, W.; Köhnlein, W.; Hutchinson, F. *Nucleic Acids Res.* **1977**, *4*, 3573–3580. Povirk, L. F.; Houlgrave, C. W. *Biochemistry* **1988**, *27*, 3850–3857. For an alternative approach based on multicomponent kinetic fitting, see: Goodisman, J.; Kirk, C.; Dabrowiak, J. C. *Biophys. Chem.* **1997**, *69*, 249.

(46) For random Poisson distribution, the average number of dsb per molecule can be calculated from the equation:  $n_2 = 1/[(f_1 + f_{II} + f_{III})/f_{III} - 1]$ . The average number of ss breaks can be determined from the fraction of supercoiled DNA remaining after irradiation  $f_1 = \exp[2(n_1 + n_2)]$ .

(47) Yoshimura, Y.; Inomata, T.; Nakazawa, H.; Kubo, H.; Yamaguchi, F.; Ariga, T. *J. Agric. Food Chem.* **1999**, *47*, 4653–4656. Rosenblum, W. I.; El-Sabban, F. Dimethyl sulfoxide (DMSO) and glycerol, hydroxyl radical scavengers, impair platelet aggregation within and eliminate the accompanying vasodilation of, injured mouse pial arterioles. *Stroke* **1982**, *13*, 35–39.

(48) Devasagayam, T. P. A.; Steenken, S.; Obendorf, M. S. W.; Schulz, W. A.; Sies, H. Formation of 8-hydroxy(deoxy)guanosine and generation of strand breaks at guanine residues in DNA by singlet oxygen. *Biochemistry* **1991**, *30*, 6283–6289.

(49) In plasmid relaxation assays at pH 6 with 15 μM of enediyne bis-lysine conjugates, no DNA was detected after electrophoresis. It might be due to the condensation of DNA, formation of complex between polycation (or its micelle) and DNA. Kircheis, R.; Wagner, E. Polycation/DNA complexes for in vivo gene delivery. *Gene Ther. Regul.* **2000**, *1*, 95–114.

(50) Alabugin, I. V.; Kovalenko, S. V. C1–C5 Photochemical Cyclization of Eneidyne. *J. Am. Chem. Soc.* **2002**, *124*, 9052–9053. Alabugin, I. V.; Manoharan, M. Radical-Anionic Cyclizations of Eneidyne: Remarkable Effects of Benzannelation and Remote Substituents on Cyclorearomatization Reactions. *J. Am. Chem. Soc.* **2003**, *125*, 4495–4509.

(51) Yang, W.-Y.; Marrone, S. A.; Minors, N.; Zorio, D. A. R.; Alabugin, I. V. Fine-tuning alkyne cycloadditions: Insights into photochemistry responsible for the double-strand DNA-cleavage via structural perturbations in diaryl alkyne conjugates. *Beil. J. Org. Chem.* **2011**, *7*, 813–823. Laroche, C.; Li, J.; Kerwin, S. M. Cytotoxic 1,2-Dialkynylimidazole-Based Aza-Enediynes: Aza-Bergman Rearrangement Rates Do Not Predict Cytotoxicity. *J. Med. Chem.* **2011**, *54*, 5059–5069.

(52) Wyllie, A. H. “Where, O death, is thy sting?” A brief review of apoptosis biology. *Mol. Neurobiol.* **2010**, *42*, 4–9, and references within.

(53) Arends, M. J.; Morris, R. G.; Wyllie, A. H. Apoptosis. The role of the endonuclease. *Am. J. Pathol.* **1990**, *136*, 593–608.

(54) Walles, S. A. S.; Zhou, R.; Liliemark, E. DNA damage induced by etoposide; a comparison of two different methods for determination of strand breaks in DNA. *Cancer Lett.* **1996**, *105*, 153–159.